PERGAMON

International Journal of Solids and Structures 38 (2001) 9149–9177

INTERNATIONAL JOURNAL OF SOLIDS and STRUCTURES

www.elsevier.com/locate/ijsolstr

Mixed mode delamination in plates: a refined approach

Domenico Bruno *, Fabrizio Greco

Department of Structural Engineering, University of Calabria, 87030 Arcavacata di Rende Cosenza, Italy

Received 1 November 2000

Abstract

Energy release rate and its mode partition in layered plates are analysed by using an improved laminated plate model. The adhesion between layers is modelled by means of a linear interface acting in the opening and sliding failure mode directions. Stress singularities at the crack tip are recovered when the stiffness of the interface approaches infinity. Kirchhoff or Reissner–Mindlin plate models are employed to describe the layers. Analytical solutions of the relevant governing equations are obtained through a variational formulation of an augmented total potential energy, in which the stiffness of the interface introduces kinematics constraints in the form of a penalty functional. Closed form solutions for energy release rates are given evidencing the effectiveness and the simplicity of the proposed model. Comparisons with fracture mechanics results—when available—are shown discussing the validity of the proposed mechanical model to predict mode partition. Interesting features emerging with the introduction of the layer-wise Reissner–Mindlin model are also highlighted, particularly with reference to coupling terms arising from shear effects.

Keywords: Laminated plates; Delamination; Interface model; Mode partition; Shear effects

1. Introduction

Failure of multilayered structures often occurs by delamination, as induced by various factors, including improper adhesion of layers, stress concentration at free edges, and low-velocity impacts. As a consequence, analysis of nucleation and propagation of separation between layers becomes essential for these structures. Accordingly, a number of approaches have been proposed, ranging between the extreme cases of fully three-dimensional analyses (Chai, 1990) and beam-like models (Kanninen, 1973; Chang et al., 1976; Chai et al., 1981; Yin and Wang, 1984; Yin et al., 1986; Allix et al., 1995). The former approaches include analyses in which an interlaminar defect grows kinking out the interface so that an energy release rate approach cannot be used (Sih, 1974). A number of simplified models have been introduced to solve particular delamination problems, based on plate theory. For example, the adhesion between the layers of a double cantilever beam scheme was modelled by means of an elastic foundation in Kanninen (1973), while a refined plate theory was used to model the layers in Chang et al. (1976). Moreover, unilateral contact

* Corresponding author. Tel.: +39-984-494027; fax: +39-984-494045.
E-mail address: d.bruno@unical.it (D. Bruno).

0020-7683/01/$ - see front matter
PII: S0020-7683(01)00179-2

approaches were utilized to analyse the delamination problem of a two-layer plate (Reddy and Grimaldi, 1985; Ascione and Bruno, 1985).

The special problem of delamination initiation and growth as induced by buckling in layered plates has been analysed from different perspectives (Chai et al., 1981; Yin et al., 1986; Yin, 1985; Bruno, 1988; Bruno and Grimaldi, 1990; Larsson, 1991; Bruno and Greco, 2000). In particular, an investigation of post-buckling effects in the modelling accuracy of delamination buckling and growth was presented by Bruno and Greco (2000). Since Griffith's criterion is often inadequate to accurately predict the growth of delamination when mixed mode loading is involved, some mixed mode fracture criteria have been proposed (see, e.g., Hutchinson and Suo, 1992). As a consequence, the problem of energy release rate mode partition becomes important. In particular, Suo and Hutchinson (1990), and Suo (1990) obtained mode decomposition by using the classical plate theory coupled with integral equations methods; whereas Schapery and Davidson (1990) and Davidson et al. (1995) completed mode decomposition derived from the classical plate theory solution by employing the finite element analysis. Mode partition was also analysed by using interface models in conjunction with simplified structural models for the layers by Allix and Corigliano (1996). Finally, a model based only on classical plate theory and containing simplified assumptions was proposed by Williams (1988).

A simple approach is presented in the present paper, where delamination growth is assumed to occur along a straight interface between layers, modelled as Kirchhoff or Reissner–Mindlin plates. In these conditions, crack growth along the interface can be analysed by means of a criterion based on the energy release rate concept. For a plane problem, in particular, the energy release rate for crack advance at the interface can be expressed as $G = G_{\mathrm{I}} + G_{\mathrm{II}}$, where the components G_{I} and G_{II} of G, are defined as the work of the normal and shear tractions acting at the interface through their respective crack face displacements when crack advances. The above mode decomposition and energy release rates definitions are an approximation for those cases in which the interfacial fracture problem predicts the classical oscillatory singularity, since the notion of G_{I} and G_{II} must be modified accordingly (Rice, 1988; Hwu and Hu, 1992; Beuth, 1996). In this context, simplifications introduced by a classical energy release rates definitions are often of secondary consequences (Hutchinson and Suo, 1992). A detailed discussion on the validity of classical energy release rates definition and on the oscillatory effects is also contained in Davidson et al. (1995).

An interface model is introduced between layers, yielding a linear relation between tractions and sliding/opening displacement jumps at the interface. A similar approach was employed by Reddy and Grimaldi (1985), and by Ascione and Bruno (1985), to solve mode I problems. In the present paper, mixed mode is investigated, together with an analysis of the influence of different kinematical assumptions on delamination behaviour. As the stiffness of the interface approaches infinity, the upper and lower layers become perfectly bonded and the shearing and opening interface tractions, corresponding to the jump displacements at the layers interface, become singular at the crack tip. It is well-known that behaviour of the above linear interface model is equivalent to that of a thin, soft, elastic layer in the limit when the layer thickness and stiffness approach zero (Bigoni et al., 1998).

The introduction of the above mentioned interface model allow us to recover energy release rates for interlaminar crack advance in a simple manner, namely, by taking the limit of the strain energy per unit interface surface at the crack tip, when interfacial stiffness approaches infinity. This procedure is shown to yield the fracture mechanics solution in the evaluation of the total energy release rate, including also the case of different layer properties and mixed mode loading conditions. Within the Kirchhoff beam-plate hypotheses, an analytical solution of the interface problem is given and algebraic expressions for mode I and II are presented. Moreover, from these results it emerges that mode partition is influenced by the assumptions made to predict interlaminar stresses. On the other hand, the analysis of the interface model coupled with the classical plate theory, is useful to evidence the main features of the interface approach. Penalty procedure convergence, estimation and behaviour of interlaminar stresses, validity of interface

model are, in fact, items of notable interest in view of the more accurate Mindlin–Reissner interface model subsequently introduced and of the extensive use of interface models in the literature. In the case of the Mindlin–Reissner plate model, a numerical solution of the relevant governing equations is given for the mode partition of the energy release rate. Moreover, when the Mindlin–Reissner plate theory is employed, an improved evaluation of shear effects on energy release rate is achieved, owing to the inclusion of coupling terms which are neglected when standard plate theories are applied. Comparisons to other shear deformation plate approaches are discussed pointing out advantages of the proposed method. The more actual shear effects included by means of a layer-wise shear deformable plate model is an interesting aspect of the present approach since, to the author's knowledge, no existing work evidences this contribution which notably enhances accuracy in energy release rate evaluation.

2. Characterization of the structural model

Let us consider a two layer-plate system as illustrated in Fig. 1, under the hypothesis of plane strain in the x–y plane. Adhesion between layers is modelled by means of a linear interface model. The layers are assumed to be homogeneous, orthotropic and linearly elastic with principal axes aligned to the global co-ordinate system and contain a plane crack with its edges aligned to the principal axis of orthotropy z, which is assumed to advance in a self similar manner in the direction of the in-plane orthotropy axis x.

The traction vector $\boldsymbol{\sigma}$ at a generic point of the interface with unit normal coincident with the y-axis can be expressed as a linear function of the jump of displacement, vector $\boldsymbol{d}$, at the interface in the form

$$\boldsymbol{\sigma} = \frac{k}{B}\boldsymbol{d}, \tag{1}$$

where $\boldsymbol{\sigma}$ has components $\boldsymbol{\sigma}_{yy}$ and $\boldsymbol{\sigma}_{yx}$ in the normal (y) and tangential (x) directions, respectively, k is the (strictly positive) stiffness coefficient for unit x-length of the interface (assumed equal in the x and y directions), the components of $\boldsymbol{d}$ are the jumps in displacement between the lower $(+)$ and the upper $(-)$ layer, $\Delta w = w^+ - w^-$ and $\Delta u = u^+ - u^-$, in the normal (y) and tangential (x) directions, respectively. Finally, B denotes the length of the plate in the z-direction. Note that the components of $\boldsymbol{\sigma}$ and $\boldsymbol{d}$ are positive when aligned with the co-ordinate axes.

The energy release rate mode components for crack advance within the interface between layers can be calculated in the context of LEFM through the strain energy stored in the interface at the crack tip. It is worth noting that perfect adhesion between layers is recovered in the limit when the interfacial stiffness approaches infinity. The mode components of the energy release rate can be calculated by means of a limit process as $k \to \infty$, with the mode I component G_{I} corresponding to opening transversal relative displacements at the crack tip (i.e. $\Delta w > 0$)

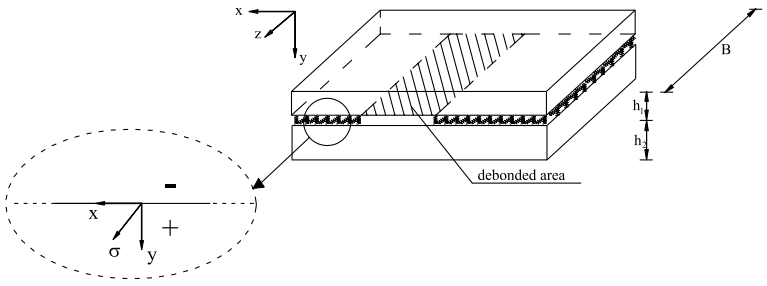

Fig. 1. Scheme of a two-layer plate bonded by a linear interface.

$$G_{\mathrm{I}} = \begin{cases} \frac{1}{B}\lim_{k\to\infty}\frac{1}{2}k\,\Delta w^2, & \text{if } \Delta w > 0 \\ 0, \text{ if } \Delta w \leqslant 0 \end{cases}, \qquad G_{\mathrm{II}} = \frac{1}{B}\lim_{k\to\infty}\frac{1}{2}k\,\Delta u^2, \tag{2}$$

where the subscript I, II denote mode I, II components and Δu and Δw refer to the delamination tip.

The specific stiffness coefficient of the interface law, k/B, can be interpreted as the stiffness of an equivalent thin layer, computed as the ratio between its elastic modulus and its thickness (Allix and Corigliano, 1996). If a sufficiently small value of the thickness is chosen, a very high k/B value is obtained perfect adhesion thus being simulated. The very high k/B value assumed in numerical calculations is of order 10^6 N/mm^3, which corresponds to assume, within common values for shear and transverse composite moduli, an equivalent layer thickness approximately of order 10^{-1} mm, $\approx$10–20 times smaller than layer thickness. In all the cases examined the chosen k/B estimate is sufficiently large to enhance accuracy of the penalty procedure but relatively small to avoid badly conditioned problems.

The meaning of Eq. (2) is that the energy released at a fixed delamination length is the work performed by stresses at the crack tip for a virtual crack extension δa. With reference to Fig. 2, the energy release rate is computed by calculating the work of interlaminar stresses $\sigma_{yy}(\delta a - \varepsilon')$ and $\sigma_{yx}(\delta a - \varepsilon')$ through displacements $\Delta w(-\varepsilon)$ and $\Delta u(-\varepsilon)$ with $0 \leqslant \varepsilon, \varepsilon' \leqslant \delta a$. The stresses considered in this procedure are obtained in the limit $k \to \infty$. On the other hand, we note that $\Delta w \to \Delta w'$, $\Delta u \to \Delta u'$ and $\varepsilon \to \varepsilon'$ in the limit $\delta a \to 0$, so that the energy release rate can be written in the form

$$\begin{aligned} G &= G_{\mathrm{I}} + G_{\mathrm{II}} \\ &= \lim_{\delta a\to 0}\lim_{k\to\infty}\frac{1}{\delta a}\int_0^{\delta a}\frac{1}{2}\sigma_{yy}(\delta a-\varepsilon)\Delta w'(\delta a-\varepsilon)\mathrm{d}\varepsilon + \lim_{\delta a\to 0}\lim_{k\to\infty}\frac{1}{\delta a}\int_0^{\delta a}\frac{1}{2}\sigma_{yx}(\delta a-\varepsilon)\Delta u'(\delta a-\varepsilon)\mathrm{d}\varepsilon. \end{aligned} \tag{3}$$

Taking into account Eq. (1) we arrive at:

$$\begin{aligned} G_{\mathrm{I}} &= \lim_{\delta a\to 0}\lim_{k\to\infty}\frac{1}{\delta a}\frac{k}{2B}\Delta w^2(\delta a-\varepsilon_0)\delta a = \frac{1}{2B}\lim_{k\to\infty} k\,\Delta w^2(0), \\ G_{\mathrm{II}} &= \lim_{\delta a\to 0}\lim_{k\to\infty}\frac{1}{\delta a}\frac{k}{2B}\Delta u^2(\delta a-\varepsilon_0)\delta a = \frac{1}{2B}\lim_{k\to\infty} k\,\Delta u^2(0), \end{aligned} \tag{4}$$

where ε_0 is an appropriate point taken between 0 and δa.

In Sections 3 and 4 both the Kirchhoff–Love and Mindlin–Reissner plate theories will be used to model the delamination of layered plates to show the influence of different kinematics assumptions on energy

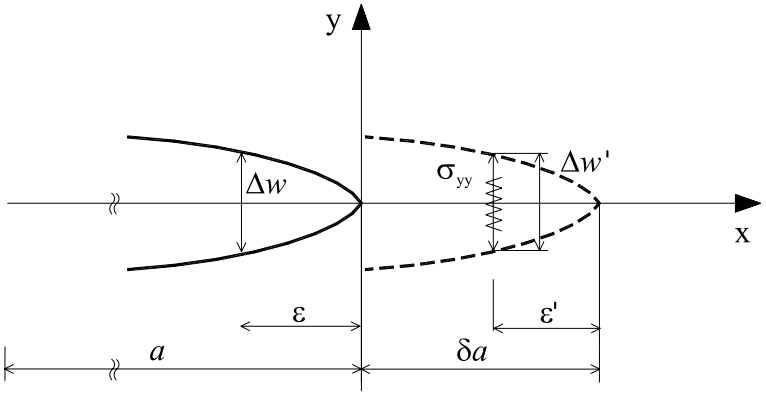

Fig. 2. Energy released for a virtual crack advance δa (mode I component).

release rate modelling. In particular, it will be shown that the use of the former and the latter kinematics leads to obtain different orders of singularity for crack tip interlaminar stresses, thus noticeably influencing energy release rate evaluation. In the latter approach, in fact, the order of singularity of interlaminar stresses arising from shear resultants at the crack tip provides an accurate shear effects evaluation in energy release rate.

3. Kirchhoff–Love plate model

A two-layers plate model is presented in Fig. 3, where the layers are assumed to be homogeneous, orthotropic and linearly elastic, with orthotropy axes aligned with the co-ordinate system. The thickness of the upper and lower layers are h_1 and h_2, respectively, and plane strain (or cylindrical bending) and clamped end conditions are assumed. The layers are characterized by Young moduli E_i along the x-axis and Poisson's ratios v^i_{xz}, v^i_{zx} along the x–z and z–x directions. We denote by $D_i = E_i B h_i^3/[12(1 - v_i^{xz} v_i^{zx})]$ and $A_i = E_i B h_i/(1 - v_i^{xz} v_i^{zx})$ the bending and axial stiffness of the ith lamina $(i = 1, 2)$, where B is the width of the plate. Isotropic properties are immediately recovered by setting $v_i^{xz} = v_i^{zx}$. Note that if bending and axial stiffness are modified accordingly, the two layers may also represent two sublaminates which individually possess midplane symmetry.

The scheme of Fig. 3, may represent a small element of a plate containing the delamination front, on which generic loads are applied, as already determined by a global plate analysis. This is the consequence of the fact that the length of the bonded plate does not affect the local solution, as we will be shown in the following. Therefore, the energy release rate and its mode partition can be evaluated for a general plate problem (including possibly geometric nonlinearities, as for instance in the case of delamination buckling (Fig. 4)) once the local stresses acting at the crack tip are given.

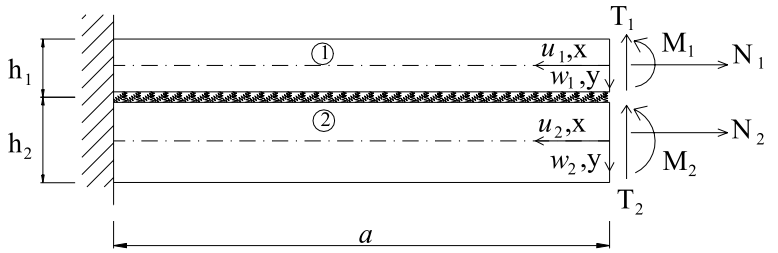

Fig. 3. Geometry and loading mode of the problem.

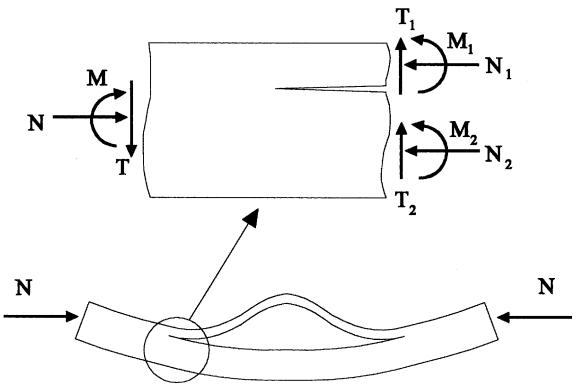

Fig. 4. Global analysis and local refined analysis scheme.

Stationarity of the total potential energy of the system is imposed to yield the governing equilibrium equations of the plate. To this purpose, the following kinematics of the two layer plate is introduced (Fig. 3):

$$\begin{cases} U_i(x,y) = u_i(x) - yw_i'(x) \\ W_i(x,y) = w_i(x) \end{cases} \quad i = 1,2, \tag{5}$$

where a prime denotes derivative with respect to the x co-ordinate and the in-plane $U_i(x,y)$ and the transverse $W_i(x,y)$ displacements of the ith layer are expressed as functions of the corresponding midsurface in-plane and transverse displacements $u_i(x)$ and $w_i(x)$, respectively. It follows from Eq. (5) that the total potential energy of the plate can be expressed in terms of the generalized displacements $u_1(x)$, $u_2(x)$, $w_1(x)$ and $w_2(x)$:

$$\begin{aligned} \Pi(u_1,u_2,w_1,w_2) = {} & \frac{1}{2}\int_0^a \left(D_1 w_1''^2 + D_2 w_2''^2 + A_1 u_1'^2 + A_2 u_2'^2\right)\mathrm{d}x + \frac{1}{2}\int_0^a \left(k\,\Delta u^2 + k\,\Delta w^2\right)\mathrm{d}x + N_1 u_1(0) \\ & - M_1 w_1'(0) + T_1 w_1(0) + N_2 u_2(0) - M_2 w_2'(0) + T_2 w_2(0), \end{aligned} \tag{6}$$

where Δu and Δw are the relative displacements at the interface:

$$\begin{aligned} &\Delta w(x) = w_2(x) - w_1(x), \\ &\Delta u(x) = U_1\left(x, \frac{h_1}{2}\right) - U_2\left(x, -\frac{h_2}{2}\right) = u_1(x) - \frac{h_1}{2}w_1'(x) - \left[u_2(x) + \frac{h_2}{2}w_2'(x)\right]. \end{aligned} \tag{7}$$

The above formulation can be understood as a stationary problem in which the constraints $\Delta u = 0$, $\Delta w = 0$ for $0 < x < a$ are introduced by means of the penalty coefficient k.

Stationarity of the functional (6) leads to the following equilibrium equations and natural boundary conditions:

$$\begin{cases} D_1 w_1^{\mathrm{IV}} + k\,\Delta u' \frac{h_1}{2} - k\,\Delta w = 0, \\ D_2 w_2^{\mathrm{IV}} + k\,\Delta u' \frac{h_2}{2} + k\,\Delta w = 0, \\ A_1 u_1'' - k\,\Delta u = 0, \\ A_2 u_2'' + k\,\Delta u = 0, \\ A_1 u_1'(0) - N_1 = 0, \\ A_2 u_2'(0) - N_2 = 0, \\ D_1 w_1'''(0) + k\,\Delta u(0)\frac{h_1}{2} + T_1 = 0, \\ D_2 w_2'''(0) + k\,\Delta u(0)\frac{h_2}{2} + T_2 = 0, \\ D_1 w_1''(0) + M_1 = 0, \\ D_2 w_2''(0) + M_2 = 0, \end{cases} \tag{8}$$

which will be utilized in the next sections.

3.1. General two-layered plate scheme

For the general case of a two-layer plate system with different mechanical and geometrical layer properties under general edge loading conditions, Eq. (8) can be solved as a homogeneous system of linear differential equations of the first order with constant coefficients reduced in terms of Δu and Δw. The system is thus reduced to an algebraic eigenvalue problem, that in general can be solved using complex analysis tools, and numerical computations are needed to obtain approximate solutions.

Eq. (8) can be rewritten in the following, useful form:

$$\begin{cases} \Delta w^{\mathrm{IV}} + \left(\frac{h_2}{2D_2} - \frac{h_1}{2D_1}\right) k\,\Delta u' + \left(\frac{1}{D_2} + \frac{1}{D_1}\right) k\,\Delta w = 0, \\ \Delta u'' - \left(\frac{1}{A_1} + \frac{1}{A_2}\right) k\,\Delta u + \left(\frac{h_2}{4} - \frac{h_1}{4}\right) \Delta w''' + \left(\frac{h_2}{4} + \frac{h_1}{4}\right) \bar{w}''' = 0, \\ \bar{w}^{\mathrm{IV}} + \left(\frac{h_2}{2D_2} + \frac{h_1}{2D_1}\right) k\,\Delta u' + \left(\frac{1}{D_2} - \frac{1}{D_1}\right) k\,\Delta w = 0, \end{cases} \tag{9}$$

where $\bar{w} = w_1 + w_2$. In addition we obtain the boundary conditions

$$\begin{cases} \Delta u(a) = 0, \\ \Delta u'(0) = \frac{N_1}{A_1} - \frac{N_2}{A_2} + \frac{M_1 h_1}{2D_1} + \frac{M_2 h_2}{2D_2}, \\ \Delta w(a) = 0, \\ \Delta w'(a) = 0, \\ \Delta w''(0) = \frac{M_1}{D_1} - \frac{M_2}{D_2}, \\ \Delta w'''(0) = \frac{T_1}{D_1} - \frac{T_2}{D_2} + \left(\frac{h_1}{2D_1} - \frac{h_2}{2D_2}\right) k\,\Delta u(0), \\ \bar{w}'''(0) = -\frac{T_1}{D_1} - \frac{T_2}{D_2} - \left(\frac{h_1}{2D_1} + \frac{h_2}{2D_2}\right) k\,\Delta u(0). \end{cases} \tag{10}$$

By introducing the vector

$$\boldsymbol{y} = \{\, \Delta u \quad \Delta u' \quad \Delta w \quad \Delta w' \quad \Delta w'' \quad \Delta w''' \quad \bar{w}''' \,\}^{\mathrm{T}},$$

Eq. (9) can be written as

$$\boldsymbol{y}' = \boldsymbol{A}\boldsymbol{y}, \tag{11}$$

where

$$A = \begin{bmatrix} 0 & 1 & 0 & 0 & 0 & 0 & 0 \\ (k/A_1) + (k/A_2) & 0 & 0 & 0 & 0 & (h_1 - h_2)/4 & -(h_1 + h_2)/4 \\ 0 & 0 & 0 & 1 & 0 & 0 & 0 \\ 0 & 0 & 0 & 0 & 1 & 0 & 0 \\ 0 & 0 & 0 & 0 & 0 & 1 & 0 \\ 0 & (kh_1/2D_1) - (kh_2/2D_2) & (-k/D_1) - (k/D_2) & 0 & 0 & 0 & 0 \\ 0 & (-kh_1/2D_1) - (kh_2/2D_2) & (k/D_1) - (k/D_2) & 0 & 0 & 0 & 0 \end{bmatrix}. \tag{12}$$

The solution for the above problem is

$$\boldsymbol{y} = \sum_{j=1}^{7} c_i \boldsymbol{u}_i\, \mathrm{e}^{\lambda_i x}, \tag{13}$$

where c_i are complex constants, $\boldsymbol{u}_i$ are the eigenvectors of the matrix $\boldsymbol{A}$, that have to be found in the complex space C^n due to the fact that $\boldsymbol{A}$ is not symmetric. Eq. (11), through relation (13), leads to

$$\boldsymbol{A}\boldsymbol{U} = \boldsymbol{U}\boldsymbol{\Lambda}, \tag{14}$$

where $\boldsymbol{U}$ is a matrix whose columns are the eigenvector components and $\boldsymbol{\Lambda}$ is a diagonal matrix whose nonzero terms are the eigenvalues λ_i.

The eigenvalue matrix can be cast in the form:

$$\boldsymbol{\Lambda} = \mathrm{diag}\{0, \alpha, -\alpha, \beta + \mathrm{i}\gamma, \beta - \mathrm{i}\gamma, -\beta + \mathrm{i}\gamma, -\beta - \mathrm{i}\gamma\},$$

where α, β, γ are real numbers and i is the imaginary unity.

As far as boundary conditions in Eq. (9) are concerned, they can be represented by the linear system:

$$\boldsymbol{U}\boldsymbol{c} = \boldsymbol{f}, \tag{15}$$

where $\boldsymbol{c}$ is the vector collecting the constants c_i, $\boldsymbol{f}$ is the vector of the rearranged boundary conditions

$$\boldsymbol{f} = \left\{0, \frac{N_1}{A_1} - \frac{N_2}{A_2} + \frac{M_1 h_1}{2D_1} + \frac{M_2 h_2}{2D_2}, 0, 0, \frac{M_1}{D_1} - \frac{M_2}{D_2}, \frac{T_1}{D_1} - \frac{T_2}{D_2}, -\frac{T_1}{D_1} - \frac{T_2}{D_2}\right\}^{\mathrm{T}},$$

and $\boldsymbol{U}$ is the matrix:

$$\boldsymbol{U} = \begin{bmatrix} u_{1,1}\,\mathrm{e}^{\lambda_1 a} & u_{1,2}\,\mathrm{e}^{\lambda_2 a} & \cdots & u_{1,7}\,\mathrm{e}^{\lambda_7 a} \\ u_{2,1} & u_{2,2} & \cdots & u_{2,7} \\ u_{3,1}\,\mathrm{e}^{\lambda_1 a} & u_{3,2}\,\mathrm{e}^{\lambda_2 a} & \cdots & u_{3,7}\,\mathrm{e}^{\lambda_7 a} \\ u_{4,1}\,\mathrm{e}^{\lambda_1 a} & u_{4,2}\,\mathrm{e}^{\lambda_2 a} & \cdots & u_{4,7}\,\mathrm{e}^{\lambda_7 a} \\ u_{5,1} & u_{5,2} & \cdots & u_{5,7} \\ u_{6,1} - u_{1,1}A_{6,2} & u_{6,2} - u_{1,2}A_{6,2} & \cdots & u_{6,7} - u_{1,7}A_{6,2} \\ u_{7,1} - u_{1,1}A_{7,2} & u_{7,2} - u_{1,2}A_{7,2} & \cdots & u_{7,7} - u_{1,7}A_{7,2} \end{bmatrix},$$

where $u_{i,j}$ is the ith component of the jth eigenvector.

The energy release rate components can be calculated numerically taking the limit for the interfacial stiffness approaching infinity. In order to avoid bad conditioning of the matrix $\boldsymbol{U}$ for large values of the interfacial stiffness, the eigensolutions with positive real part can be excluded from the solution. These, in fact, do not affect the solution, because the constants c_i must approach zero in the limit process, otherwise the relative component solutions $\boldsymbol{y}_i$ approach infinity along the plates. In fact, the corresponding eigenvalues approach infinity and only those with a negative real part must be utilized in Eq. (13) in the numerical penalty procedure.

The computed value for the total energy release rate agrees well also at low relative value of the interlaminar stiffness with the value obtained applying the J-integral concept (Yin and Wang, 1984) or by energy argumentation (Suo and Hutchinson, 1990).

The convergence of the energy release rate to the limit value $k \to \infty$ is shown in Fig. 5a for a delaminated plate subjected to two opposite moments in terms of the dimensionless total energy release rate G_T/E_1T and its mode components G_{I}/E_1T, G_{II}/E_1T, where T is the thickness of the whole plate. Layers are assumed as isotropic plates and the following essential data parameters are used:

$$h_1 = 10 \text{ mm}, \quad E_1 = 100.000 \text{ MPa}, \quad B = 50 \text{ mm}, \quad M = 100.000 \text{ Nmm}.$$

The relative error for the total energy release rate computed with the present approach and that obtained with the J-integral method is of about 10^{-12} percent in the whole range of the parameter k/E_1. The solution is obtained through the simplified method in which the positive eigenvalues of the solution are excluded. Therefore, the solution is not affected by the length of the bonded part of the plate (i.e. a).

The convergence to the limit value $k \to \infty$ is analysed in Fig. 5b by using the complete solution. It can be noted that in this case badly conditioned problems are experienced for k/B values larger than 3.5×10^6. Substantially, the same behavior of the solution obtained by excluding positive real part eigenvalues is shown.

Interlaminar stresses for an asymmetrical two-layer plate system are reported in Fig. 6. Different values of the dimensionless interfacial stiffness k/E_1 are considered ranging in geometric progression from 0.0081 to 1. As the interlaminar stiffness coefficient k approaches infinity, shear and normal interlaminar stresses assume a singular behaviour at the crack tip while they vanish along the perfectly bonded interface. With the exception of the singular behaviour of the small element containing the crack tip (in which interlaminar

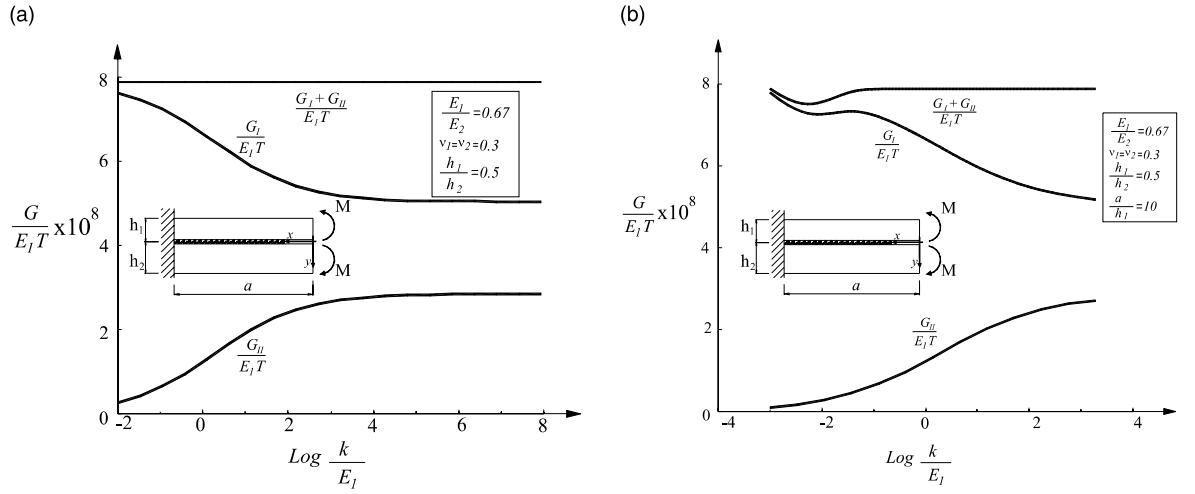

Fig. 5. Convergence of the solution for increasing values of k/E_1: (a) simplified solution, (b) complete solution.

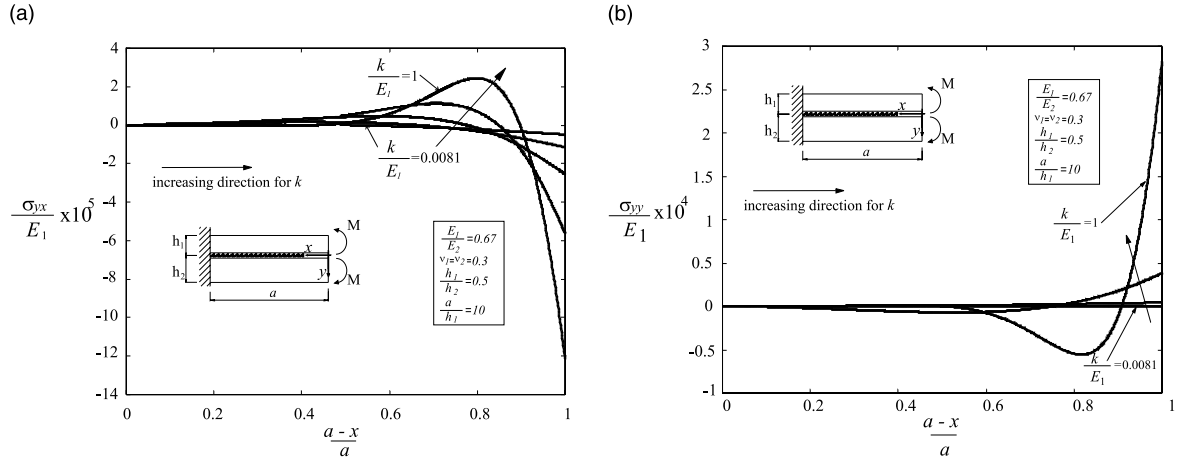

Fig. 6. Plot of interlaminar shear (a) and normal (b) stresses for increasing k/E_1. Complete solution.

normal stresses are equivalent to a couple equilibrating the external applied bending moment), the remaining two-layer plate behaves like an unstressed layer, being the loading system self-equilibrated.

3.2. Solution of the simplified two-layer plate scheme

When the simple symmetrical two-layers plate scheme is considered and the same mechanical and geometrical characteristics are assumed for the layers (i.e. $h_1 = h_2 = h$, $A_1 = A_2 = A$ and $D_1 = D_2 = D$), a closed-form solution of Eq. (9) can be obtained. In fact, under the above-mentioned simplified hypotheses, the equations for Δu and Δw may be decoupled. This analytical solution will be obtained below and is thought to be important to understand the essential features of the problem.

The mode I energy release rate can be computed by using the first term of Eq. (2), after solution of Eq. (9), involving the opening displacement Δw. It is possible to show that the latter is

$$\Delta w(x) = e^{-\alpha x}[c_1 \sin(\alpha x) + c_2 \cos(\alpha x)] + e^{\alpha x}[c_3 \sin(\alpha x) + c_4 \cos(\alpha x)], \tag{16}$$

where $4\alpha^4 = 2k/D$. The coefficients c_i are given in Appendix A.

In the limit $\alpha \to \infty$, the vertical displacement jump Δw at the interface tends to zero, while the interlaminar stresses $\sigma_{yy} = k\,\Delta w/B$ cancel out on the whole length, except at the delamination tip, where a stress singularity is present. The above behavior is represented in Fig. 7, with the following geometrical and mechanical data parameters of the isotropic layers:

$$E = 145.000 \text{ MPa}; \quad \nu_{xz} = \nu_{zx} = 0.3; \quad T_1 = T = 40 \text{ N}; \qquad T_2 = -T = -40 \text{ N}; \quad \ell = 50 \text{ mm};$$
$$a = 200 \text{ mm}; \quad B = 30 \text{ mm}; \quad h = 5 \text{ mm};$$

where ℓ is the length of layers along the debonded interface. Several values of the dimensionless interlaminar stiffness k/E are considered ranging in geometric progression from 6.9×10^{-6} to 6.9×10^{-2}. It may be noted from Figs. 7 and 8, that the stresses near the crack tip tend to a point force and a point couple as $k \to \infty$.

From Eq. (16) the expression for $\Delta w(0)$ may be obtained, thus G_I may be evaluated through first term of Eq. (2) leading to:

$$G_I = \frac{m^2 D}{4B} = \frac{(M_1 - M_2)^2}{4DB}. \tag{17}$$

The above results, although referred to a particular scheme, underline some essential characters of the proposed interface model both in the prediction of interlaminar stresses behaviour and in the evaluation of energy release rate. In particular, it can be observed that no shear effects are introduced in energy release rate evaluation as a consequence of this particular modelling of interlaminar stresses singularity at the crack tip. In fact, by use of Eq. (16) in conjunction with Eq. (1) and the first of Eq. (2), it can be shown that interlaminar normal stress terms arising from shear loading conditions (i.e. those containing the t factor

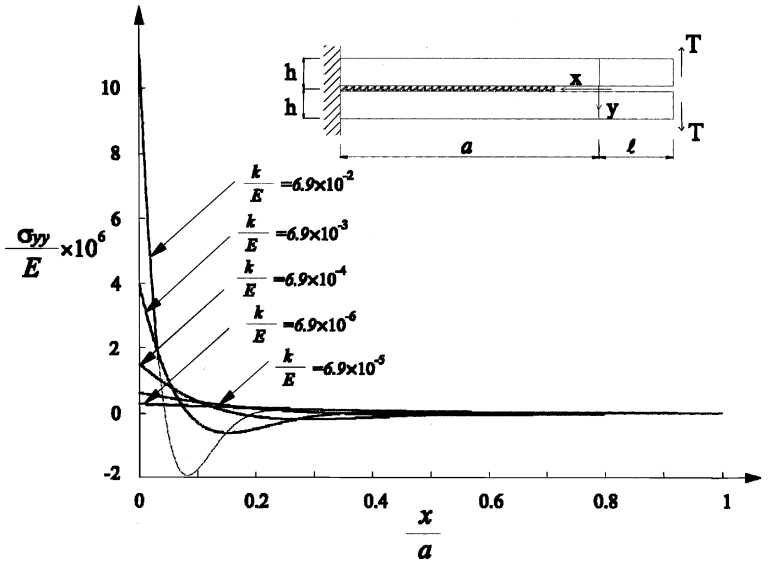

Fig. 7. Interlaminar normal stress σ_{yy}/E for increasing values of k/E.

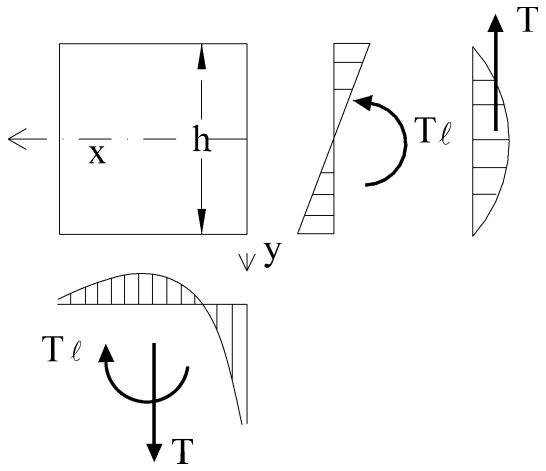

Fig. 8. Equilibrium sketch at the crack tip (mode I loading).

introduced in the Appendix A) go to infinity slower than α^2 as $\alpha \to \infty$ while only interlaminar normal stress terms of order α^2 give contribution to the energy release rate G_{I}.

The mode II energy release rate is now evaluated below through the second term of Eq. (2). Therefore Eq. (9), must be used to obtain the relative displacement Δu, which, after some computation, can be written in the form:

$$\Delta u = \frac{h}{2\beta^2} c_1 + c_2 \mathrm{e}^{\beta x} + c_3 \mathrm{e}^{-\beta x}, \tag{18}$$

where the coefficients c_i are given in Appendix B.

The effects of the sliding mode loading condition are considered in Figs. 9 and 10, where the shearing interlaminar stresses tend to the constant value $3/4(T_1 + T_2)/Bh$ for $0 < x \leqslant a$ and to a singular value for $x = 0$ to equilibrate the resultant of the longitudinal stresses in the cross sections at the crack tip (see the sketch in Fig. 10). The geometrical and mechanical parameters involved in this example are the same employed to investigate the opening mode, with $T_1 = T_2 = T = -40$ N.

Using the second term of Eq. (2) and Eq. (18) the mode II energy release rate component becomes:

$$G_{\mathrm{II}} = \frac{A}{16B}\left[\frac{N_1 - N_2}{A} + \frac{h(M_1 + M_2)}{2D}\right]^2. \tag{19}$$

The above results coincide with those obtained by Suo and Hutchinson (1990), and Schapery and Davidson (1990). In the case of the double cantilever beam (DCB) geometrical scheme with general loading mode these conclusion are also in agreement with the results obtained by Williams (1988) because from Eqs. (17) and (19) we can see that the mode I component arises from opposite moments, while the mode II component is related to a mismatch of axial force and to moments of the same sign. As will become clear in the following, this holds true only for this particular scheme where layers have the same geometrical and mechanical parameters.

Moreover, it emerges from the above-introduced formulas that shear forces, as expected, do not affect the energy release rate value.

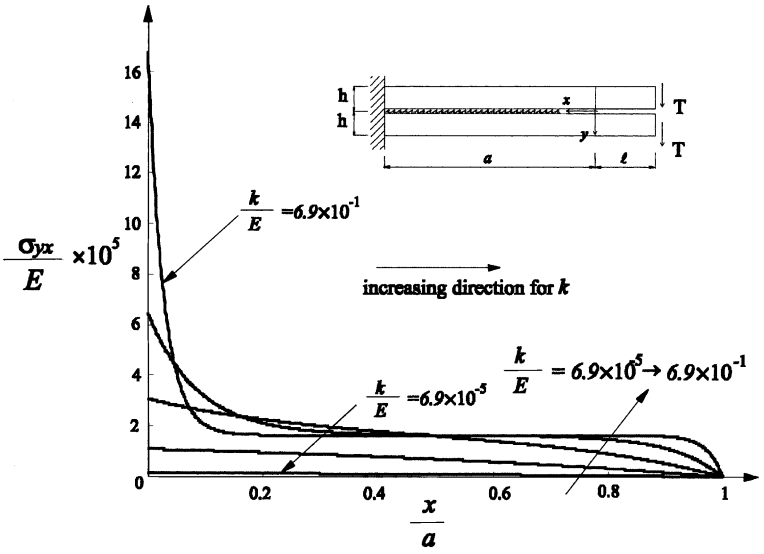

Fig. 9. Interlaminar shearing stress σ_{yx}/E for increasing values of the penalty parameter k.

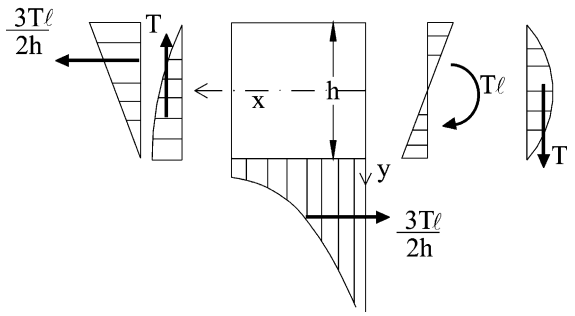

Fig. 10. Equilibrium sketch at the crack tip (mode II loading).

3.3. Energy release rate mode partition

The analytical solution of the cracked two-layer plate, can now be used to investigate the effects of the loading system on the energy release rate mode partition. This is useful to illustrate the main characteristics of the linear interface model based on the classical plate theory.

Energy release rate G can be calculated with the aid of the J-integral concept. Extending the solution reported in Yin and Wang (1984), to the case of different materials for the layers, we obtain the following expression for the energy release rate G in terms of bending and axial stresses at the crack tip:

$$G = \frac{1}{2B}\left[\frac{(N^*)^2}{A_1} + \frac{(N^*)^2}{A_2} + \frac{(M^u)^2}{D_1} + \frac{(M^l)^2}{D_2}\right], \tag{20}$$

where N^*, M^l, M^u, is the only stress resultant subsystem that produces a singular stress field (see Fig. 11). Eq. (20) is obtained by applying the J-integral along a closed path with vertical segments across the layers (see scheme (b) in Fig. 11).

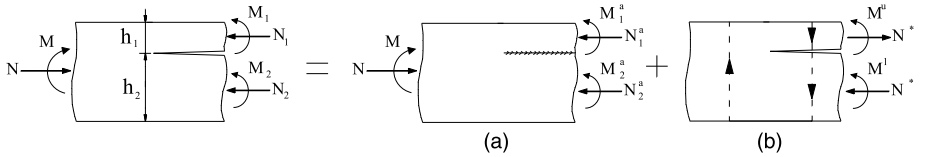

Fig. 11. Stress resultant decomposition at the crack tip.

The first ineffective (i.e. which does not produce energy release rate) subsystem is obtained by using equilibrium requirements and matching crack tip longitudinal strains and curvatures of the upper and lower layers. The expressions for axial loads and bending moments are given in Appendix C.

On the other hand, the effective subsystem (b) leading to energy release rate, is determined by the following formulas:

$$\begin{aligned} N^* &= N_1^a - N_1, \\ M^u &= M_1 - M_1^a, \\ M^l &= M_2 - M_2^a. \end{aligned} \tag{21}$$

To obtain the energy release rate partition we must decompose the equivalent stress system (b) in such a way that G does not contain any mixed product terms between mode I and mode II stress resultants. To this end, a loading condition is necessary, giving a pure mode delamination. Accordingly, the equivalent bending moments can be decomposed into its mode component (see Fig. 12):

$$\begin{aligned} M^u &= M_{\mathrm{I}}^u + M_{\mathrm{II}}^u, \\ M^l &= M_{\mathrm{I}}^l + M_{\mathrm{II}}^l = \alpha M_{\mathrm{I}}^u + \beta M_{\mathrm{II}}^u, \end{aligned} \tag{22}$$

while, the corresponding axial terms N_{I}^* and N_{II}^* can be easily evaluated by the aid of equilibrium requirements. We obtain therefore the following expressions:

$$G_{\mathrm{I}} = \frac{1}{2B}\left\{ \frac{M_{\mathrm{I}}^{u2}}{D_1} + \frac{\alpha^2 M_{\mathrm{I}}^{u2}}{D_2} + \left[\frac{2(1+\alpha)M_{\mathrm{I}}^u}{h_1+h_2}\right]^2 \left(\frac{1}{A_1}+\frac{1}{A_2}\right)\right\}, \tag{23}$$

$$G_{\mathrm{II}} = \frac{1}{2B}\left\{ \frac{M_{\mathrm{II}}^{u2}}{D_1} + \frac{\beta^2 M_{\mathrm{II}}^{u2}}{D_2} + \left[\frac{2(1+\beta)M_{\mathrm{II}}^u}{h_1+h_2}\right]^2 \left(\frac{1}{A_1}+\frac{1}{A_2}\right)\right\}, \tag{24}$$

under the condition that the mixed product terms between mode I and mode II stress resultants:

$$G_{\mathrm{I,II}} = \frac{1}{2B}\left\{ \frac{2M_{\mathrm{I}}^u M_{\mathrm{II}}^u}{D_1} + \frac{2\alpha\beta M_{\mathrm{I}}^u M_{\mathrm{II}}^u}{D_2} + \frac{8(1+\alpha)(1+\beta)M_{\mathrm{I}}^u M_{\mathrm{II}}^u}{(h_1+h_2)^2}\left(\frac{1}{A_1}+\frac{1}{A_2}\right)\right\} \tag{25}$$

vanish. Now we can define the expressions for α and β. The partitioned bending moments of the upper layer M_{I}^u, M_{II}^u can be expressed in terms of the global equivalent stresses M^u, M^l by solving the system (22):

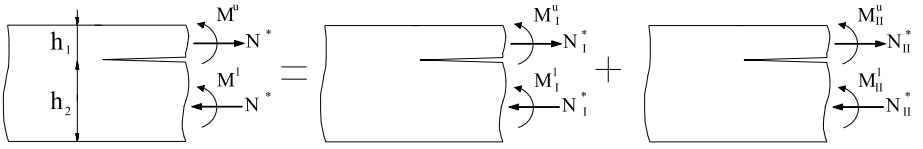

Fig. 12. Partition of the effective loading system.

$$M_{\mathrm{I}}^{u}=\frac{-\beta M^{u}+M^{l}}{\alpha-\beta},\quad M_{\mathrm{II}}^{u}=\frac{\alpha M^{u}-M^{l}}{\alpha-\beta}. \tag{26}$$

Extensive numerical calculations obtained by applying different loading conditions to the proposed interface model have demonstrated that the pure mode I condition is represented by two moments that produce the same strain at the crack tip. Thus, using this condition leads to the following relation for α:

$$\alpha=\frac{\bar{\alpha}M_1-M_2^a}{M_1-M_1^a}=-\frac{D_1h_2^2+D_2h_1(4h_1+3h_2)}{D_2h_1^2+D_1h_2(3h_1+4h_2)}. \tag{27}$$

Details of calculations leading to Eq. (27) are given in Appendix C.

On the other hand, β is obtained by imposing the condition that Eq. (25) must be equal to zero:

$$\beta=\frac{h_2}{h_1}. \tag{28}$$

A limited numerical analysis, showing the convergence of the linear interface model to Eqs. (23) and (24), is reported in Fig. 13, where a cracked plate composed of two isotropic layers, subjected to two opposite moments ($M_2=-M_1=100$ Nm) and two opposite axial forces ($N_2=-N_1=0.1$ MN) is considered. Other numerical calculations have been made with many different loading conditions leading to the same conclusion.

A comparison between our approach and those proposed by Suo (1990), and by Williams (1988) is shown in Fig. 14, for a homogeneous isotropic plate with an asymmetric crack. Suo's results are extracted from his approximated equation (17), which refers to the same problem solved by Suo and Hutchinson (1990). As can be noted from Fig. 14 the curve obtained by using the approach presented in Williams (1988) shows a great amount of mode I energy release rate and for $M_2/M_1=-1$ only mode I is present. The hypotheses introduced in Williams (1988) lead to very approximate results due to the fact that Williams' analysis is based on the simplified assumption that for arbitrary geometrical and material layer properties, opposite moments always cause only mode I energy release rate component and axial forces give only mode II energy release rate component.

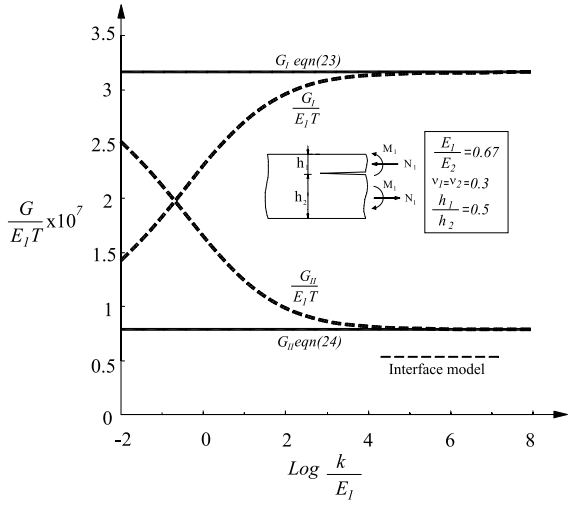

Fig. 13. Convergence of the energy release rate components to Eqs. (23) and (24) for a mixed mode loading system, as a function of the penalty parameter k.

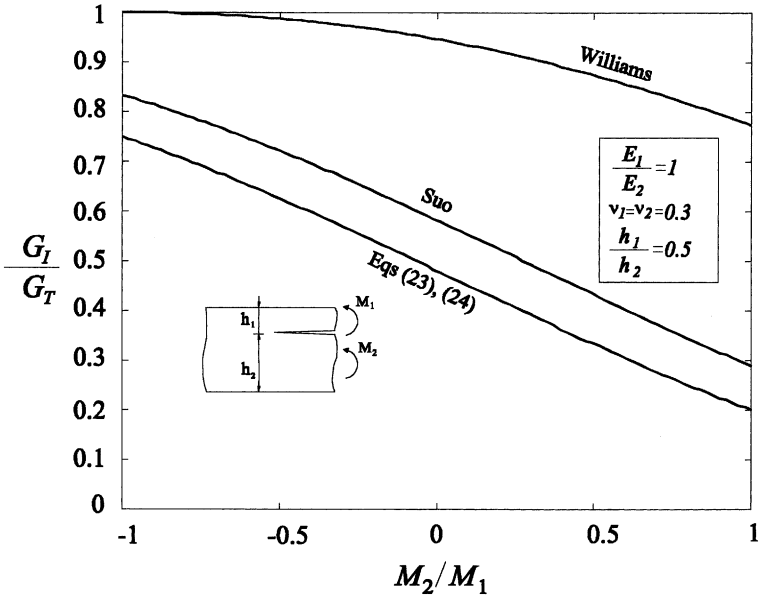

Fig. 14. Comparison of energy release rate modes prediction between our approach and that of Williams (1988), and Suo (1990). Asymmetric two-layer plate subjected to end moments.

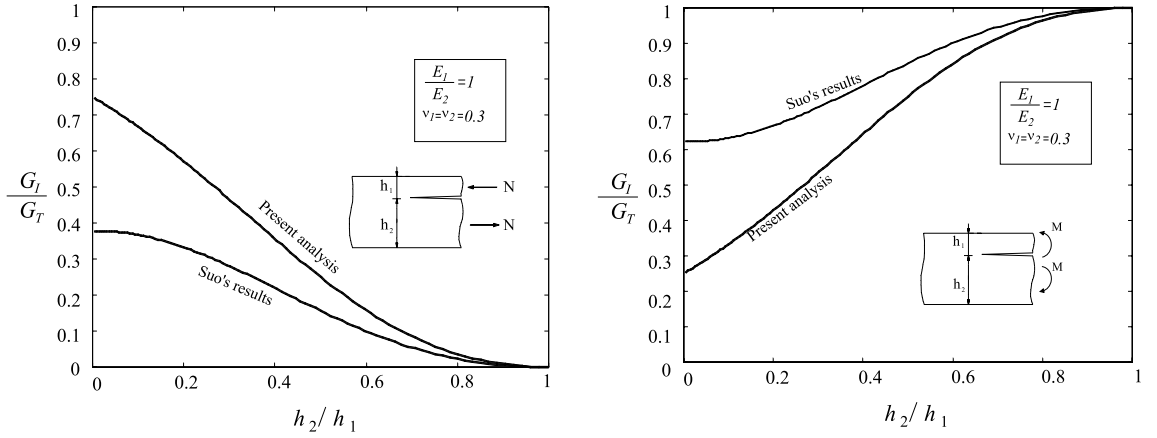

Fig. 15. Comparison of energy release rate modes prediction between interface model approach and that of Suo (1990) for different values of h_2/h_1 thickness ratio. Asymmetric two-layer plate subjected to opposite axial forces and end moments.

The comparison for different values of h_1/h_2 ratio is presented in Fig. 15. It can be noted that the larger differences between plotted results occur for the thin film model (i.e. $h_1/h_2 \to 0$). In fact, when the plate deformation assumptions are concerned, in the case of two applied opposite axial forces a greater amount G_{I} is activated, while in the case of opposite end moments a greater amount of G_{II} is activated.

Davidson et al. (1995) found a good agreement with Suo's results by using an accurate approach in which the finite element method was employed to complete mode decomposition from the classical plate theory solution. Thus, comparisons in Figs. 14 and 15 are useful to evidence the influence of the different

assumptions made to reconstruct interlaminar stresses. Interface models, although incorporating some approximations inherent in the plate scheme, lead to solutions which are able to capture the main features of the problem and to give a synthetic understanding of the mechanical delamination behavior of layered systems. In addition, interface models provide an easy way to account for energy release rate mode components interaction in delamination problems of more complex plate geometry (multiple delaminations, delamination buckling, etc.). In fact, they are frequently used in the literature both in numerical and analytical approaches (Allix and Corigliano, 1996; Allix et al., 1995; Ascione and Bruno, 1985; Reddy and Grimaldi, 1985) and will be utilized in the next section to include shear effects which may notably influence delamination behavior.

Differences emerging from comparisons shown in Figs. 14 and 15 related to the energy release rate mode I and mode II components ratio (not in the total amount of energy released) are due to the different assumptions made to take into account for local effects at the crack tip within the classical beam-plate theory. As a matter of fact, in our approach the energy release rate modes are recovered by using an interface model with the classical plate model, while the classical plate model is adopted in Suo and Hutchinson (1990), Suo (1990), Schapery and Davidson (1990) and Davidson et al. (1995) only to obtain the total energy release rate, and for mode partition a local continuum analysis is needed. In particular in the latter case, the local continuum analysis is developed by referring to a semi-infinite crack scheme under remote edge loading. The above mentioned continuum analysis, removing the beam-plate kinematics assumptions at the crack tip zone, provides an accurate estimation of crack tip stresses in the context of the classical plate theory. On the other hand, these continuum based approaches do not include shear effects in energy release rate evaluation, whereas the interface model here proposed can be easily improved to take into account for layers shear deformability, providing a simple interpretation of the relevant quantities which govern energy release rate. To this aim, the reconstruction of local stresses will be improved in the next paragraph where shear effects will be introduced by using a shear deformable layer-wise plate model.

4. Reissner–Mindlin plate model

The delaminated two-layer plate model is now refined by using the Reissner–Mindlin kinematics for the layers coupled with the above-described linear interface model. The shear deformability of the plate is accounted for by introducing the shear stiffness parameters $A_i^* = K_i G_i^{xy} B h_i$ of the ith layer, G_i^{xy} and K_i being the shear modulus and the shear correction factor of the ith layer, respectively. Additional details about the choice of an optimal shear correction factor can be found in Chatterje and Kulkarni (1979). In our numerical calculations K_i is always set equal to $5/6$. The importance of shear deformations in composite laminates is well-known; as a matter of fact, laminates exhibit lower shear to axial modulus ratio than isotropic materials, so that it becomes very important to analyse the effect of shear deformations on energy release rate evaluation. With the refined approach proposed here it becomes possible to investigate shear effects on energy release rate. As will be shown in the following, these effects produce, in addition to standard shear terms included if a classical Reissner–Mindlin beam-plate theory is adopted, new contributions leading to a much larger relative shear influence in energy release rate evaluation. The accurate analyses provided by Schapery and Davidson (1990) and Suo (1990) being based on classical plate theory, can not be used to give effective comparisons in the case of a shear deformable plate model. This, eventually, will be assessed through considerations based on a more actual prediction of deformation mechanism obtained with the proposed approach in comparison with other shear deformation theories.

With reference to Fig. 3, the following kinematics assumptions are used for the ith layer:

$$\begin{cases} U_i(x,y) = u_i(x) + y\psi_i(x), \\ W_i(x,y) = w_i(x). \end{cases} \tag{29}$$

It follows that the stationary condition of the total potential energy yields the following equilibrium equations and natural boundary conditions:

$$\begin{cases} D_1\psi_1'' - A_1^*(\psi_1 + w_1') + k\,\Delta u\frac{h_1}{2} = 0, \\ D_2\psi_2'' - A_2^*(\psi_2 + w_2') + k\,\Delta u\frac{h_2}{2} = 0, \\ A_1^*(\psi_1' + w_1'') + k\,\Delta w = 0, \\ A_2^*(\psi_2' + w_2'') - k\,\Delta w = 0, \\ A_1 u_1'' - k\,\Delta u = 0, \\ A_2 u_2'' + k\,\Delta u = 0, \\ A_1 u_1'(0) - N_1 = 0, \\ A_2 u_2'(0) - N_2 = 0, \\ A_1^*\big(\psi_1 + w_1'\big)(0) - T_1 = 0, \\ A_1^*\big(\psi_2 + w_2'\big)(0) - T_2 = 0, \\ D_1\psi_1'(0) - M_1 = 0, \\ D_2\psi_2'(0) - M_2 = 0, \end{cases} \tag{30}$$

where

$$\begin{aligned} &\Delta w(x) = w_2(x) - w_1(x), \\ &\Delta u(x) = u_1(x) + \frac{h_1}{2}\psi_1(x) - \left[u_2(x) - \frac{h_2}{2}\psi_2(x)\right]. \end{aligned} \tag{31}$$

The limit for k approaching infinity of the solution sequence of Eq. (30), now depends on the length of the uncracked plate a. This reflects the layer-wise kinematics assumptions which includes shear deformation by distinguishing section rotation from midplane layer slope in each layer. In fact, the constraint of zero relative displacements at the interface, imposed in the form of a penalty formulation, does not lead to null relative section rotations between layers along the uncracked plate, due to shear deformations (the cancellation of the derivative $\mathrm{d}\Delta w/\mathrm{d}x$ of the relative transverse displacement for $0 \leqslant x < a$ being only implied). Thus, the uncracked plate cannot be regarded as a unique composite plate due to the difference in section rotations. Note that the penalty formulation of interface constraint is necessary to capture singular or discontinuous behaviour of displacement derivatives and interlaminar stresses. Roughly speaking, this can be explained since the penalty solution of the constrained minimization problem, under some regularity conditions, provides convergence to the minimum solution in the space containing displacement functions whose first derivatives are square-integrable (in particular, piece-wise continuous) in $(0, a)$ and interlaminar stress functions that are square-integrable in $(0, a)$ (piece-wise continuous). This can be proved within the Lagrange multiplier method, of which the penalty approach constitutes an alternative (see Reddy, 1986). The energy release rate evaluation depends on the a/h_i ratio; only if we assume that this ratio is much greater than unity, the solution is practically unaffected by the essential boundary conditions (i.e. at $x = a$). Under this hypothesis, our model can be applied in the context of a local analysis (i.e. for a plate segment in the neighbourhood of the delamination tip) for a general delamination problem by using the global analysis results. This kind of assumptions is coherent if we use a plate theory to predict energy release rate: here the equivalence between a local J-integral computation and a global energy approach can be assessed (see Bruno and Greco, 2000, where examples show the analytical equivalence between the local approach and the global energy approach).

At first, in order to evidence the main features of the proposed approach, a simplified plate scheme is presented, subsequently, these features will be analysed with reference to the general solution.

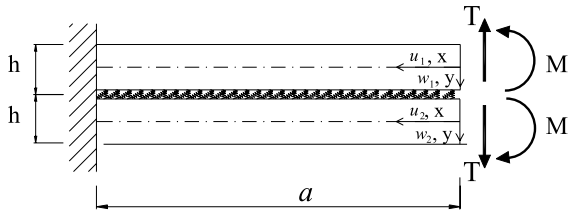

Fig. 16. Geometry and loading mode of the double cantilever model.

4.1. Simple two-layer plate system scheme

With reference to the simple symmetric two-layer plate system scheme ($h_1 = h_2 = h$, $A_1 = A_2 = A$, $A_1^* = A_2^* = A^*$ and $D_1 = D_2 = D$) shown in Fig. 16, in the case of symmetric loading condition it is possible to get an analytical solution. The relevant governing equations can be written as

$$\begin{cases} A^*(\psi_1' + w_1'') - 2kw_1 = 0, \\ A^*\left(\psi_1 + w_1'\right) - D\psi_1'' = 0, \end{cases} \tag{32}$$

with the following boundary conditions:

$$\begin{cases} w_1 = 0,\ \psi_1 = 0, \\ D\psi_1'(0) = M,\ A^*\left(\psi_1 + w_1'\right)(0) = T. \end{cases} \tag{33}$$

Similarly to Section 3.1, the above boundary value problem can be solved by reducing the system of second order linear differential equations to a homogeneous system of linear differential equations of the first order. Assuming $\boldsymbol{y} = \left\{w_1, w_1', \psi_1, \psi_1'\right\}^{\mathrm{T}}$, the linear operator $\boldsymbol{A}$ becomes

$$\boldsymbol{A} = \begin{bmatrix} 0 & 1 & 0 & 0 \\ 2k/A^* & 0 & 0 & -1 \\ 0 & 0 & 0 & 1 \\ 0 & A^*/D & A^*/D & 0 \end{bmatrix}. \tag{34}$$

The solution of $\boldsymbol{y}' = \boldsymbol{A}\boldsymbol{y}$ has the form $\boldsymbol{y} = \sum_{j=1}^{4} c_i \boldsymbol{u}_i \mathrm{e}^{\lambda_i x}$ and the boundary conditions can be rewritten in the form $\boldsymbol{U}\boldsymbol{c} = \boldsymbol{f}$, where

$$\boldsymbol{U} = \begin{bmatrix} u_{1,1}\,\mathrm{e}^{\lambda_1 a} & u_{1,2}\,\mathrm{e}^{\lambda_2 a} & u_{1,3}\,\mathrm{e}^{\lambda_3 a} & u_{1,4}\,\mathrm{e}^{\lambda_4 a} \\ u_{2,1} + u_{3,1} & u_{2,2} + u_{3,2} & u_{2,3} + u_{3,3} & u_{2,4} + u_{3,4} \\ u_{3,1}\,\mathrm{e}^{\lambda_1 a} & u_{3,2}\,\mathrm{e}^{\lambda_2 a} & u_{3,3}\,\mathrm{e}^{\lambda_3 a} & u_{3,4}\,\mathrm{e}^{\lambda_4 a} \\ u_{4,1} & u_{4,2} & u_{4,3} & u_{4,4} \end{bmatrix}, \tag{35}$$

while $\boldsymbol{f} = \{0, T/A^*, 0, M/D\}$.

The eigenvalue matrix of $\boldsymbol{A}$ can be expressed as $\boldsymbol{\Lambda} = \mathrm{diag}\{\alpha, -\alpha, \beta, -\beta\}$ where

$$\alpha = \sqrt{\frac{Dk - \sqrt{Dk(Dk - 2A^{*2})}}{A^*D}} \quad \text{and} \quad \beta = \sqrt{\frac{Dk + \sqrt{Dk(Dk - 2A^{*2})}}{A^*D}}.$$

Since we are interested in the behaviour of the solution as $k \to \infty$ we note that $\lim_{k\to\infty} \alpha = \sqrt{A^*/D}$ and $\lim_{k\to\infty} \beta = \infty$. If we suppose that the length of the bonded plate a is much greater than h (as in the case of an infinitely long plate), the only meaningful eigenvalues become the negative ones, so that the energy release rate can be computed by utilizing only the terms of the solution associated with $-\alpha$, $-\beta$. If we

indicate these two negative eigenvalues with $\lambda_{1,2}$, it is found that the energy release rate becomes (due to the symmetry of the problem only mode I is involved):

$$G_{\mathrm{I}} = \lim_{k\to\infty} \frac{1}{2B} k \Delta w(0)^2 = \lim_{k\to\infty} \frac{1}{2B} k \left(2 \sum_{i=1,2} c_i u_{1i} \right)^2 = \frac{M^2}{DB} + \frac{T^2}{A^* B} + \frac{2MT}{B\sqrt{A^* D}}. \tag{36}$$

It can be seen from Eq. (36) that two new terms appear in the energy release rate expression, when compared to the Kirchhoff–Love beam-plate model (Eq. (17)). The first term T^2/BA^* arises from the difference between the strain energy stored (per unit length) in the plate due to shear stresses ahead and behind the crack tip, while the second $2MT/B\sqrt{A^*D}$ arises from the shear/bending interaction at the crack tip.

The same result can be obtained by applying the J-integral concept. To this end we consider first the approximate Kirchhoff–Love plate model, thus obtaining:

$$J = \oint_C \left(-\frac{1}{2}\sigma_{ij}\varepsilon_{ij} - \sigma_{ij} n_j \frac{\partial u_i}{\partial x} \right) \mathrm{d}s = \oint_C \left(\frac{1 - \upsilon_{zx}\upsilon_{xz}}{E_x} \sigma_x^2 + \frac{\sigma_{xy}^2}{G_{xy}} \right) \mathrm{d}y = \frac{M^2}{DB} + \frac{T^2}{A^* B}, \tag{37}$$

where the path C is the rectangle (ABCDEF) surrounding the crack tip (see Fig. 17).

If we consider now the interface model with the Mindlin kinematics, the following result is arrived:

$$\lim_{k\to\infty} w_1'(0) = \frac{M}{\sqrt{A^* D}} + \frac{T}{A^*}, \quad \lim_{k\to\infty} \psi_1(0) = -\frac{M}{\sqrt{A^* D}}. \tag{38}$$

Therefore, if an end couple is applied, the function w_1' goes to zero for $0 < x \leqslant a$, with a discontinuity at $x = 0$, while ψ_1 tends toward the function $\psi_1(0)\exp(-\sqrt{A^*/D}x)$. Moreover, the interlaminar stresses decay along the length of the bonded beam. On the other hand, if only a shear force T is applied, w_1' exhibits similar behavior, but ψ_1 is identically zero for every x and interlaminar stresses are zero for $0 < x \leqslant a$. Applying the J-integral technique to path C, but now with the vertical segment CD behind the crack tip so far that we can assume $\psi_1 = 0$, leads to:

$$J = \int_{-h/2}^{h/2} \left(\frac{1 - \upsilon_{zx}\upsilon_{xz}}{E_x} \sigma_x^2 + \frac{\sigma_{xy}^2}{G_{xy}} \right) \mathrm{d}y - 2 \int_{-h/2}^{h/2} \sigma_{xy} \psi_1(0) \mathrm{d}y = \frac{M^2}{BD} + \frac{T^2}{BA^*} + 2\frac{MT}{B\sqrt{A^* D}}, \tag{39}$$

where it is apparent that the coupling term $2MT/B\sqrt{A^*D}$ arises from the discontinuity of the end rotation between the two section enclosing the crack tip.

It can be observed from above results that the influence of shear cannot be limited only to the standard term T^2/BA^*, but the cross term $2MT/B\sqrt{A^*D}$ must also be accounted for. This is due to the shear/bending

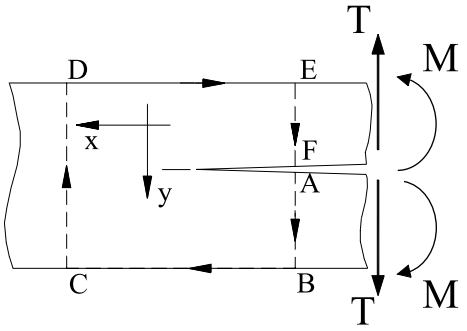

Fig. 17. Integration path around the crack tip.

interaction, an effect which may have important consequences on the energy release rate value, especially for slender laminates. In fact, the ratio between the coupling and shear term is proportional to $2(M/Th)(12G_{xy}/E_{xx})^{1/2}$ which may be larger than unity because a low $(G_{xy}/E_{xx})^{1/2}$ (approximately between $1/5$ an $1/7$ for laminates having a longitudinal to shear modulus ratio between 20 and 50) value may be compensated by a very high M/Th value (approximately between 10 and 20).

The above results are still coherent even in the context of a 2-D continuum analysis. If we think of T and M in this case as two different load systems for this mode I problem and due to linearity, we can express the total stress intensity factor as $K_{\mathrm{I}}^{T} + K_{\mathrm{I}}^{M}$, related to the shear force T and bending moment M. Since the energy release rate is proportional to the square of the stress intensity factor K_{I}, it follows that a cross product term $K_{\mathrm{I}}^{T}\ K_{\mathrm{I}}^{M}$ must come into play.

The behaviour of the energy release rate is investigated in Fig. 18, where a comparison is proposed between results obtained from the complete solution (i.e. without excluding the positive eigenvalues) of the interface model as the a/h ratio increases, and those corresponding to Eqs. (36) and (37). Moreover, the convergence of the solution for increasing stiffness parameter to the asymptotic value of Eq. (36) is shown. The following mechanical, geometrical and loading parameters are used:

$$h = 1 \text{ mm},\ E = 140.000 \text{ MPa},\ \nu_{xz} = \nu_{zx},\ \ell = 10 \text{ mm},\ T = 200 \text{ N},\ B = 20 \text{ mm}.$$

We can note that for high values of the a/h and k/E ratios, the numerical energy release rate value practically equals that computed from Eq. (36). Moreover, the cross product term has a significant effect on the energy release rate evaluation. Compared to the bending energy release rate, the shear part is equal to the 5.13% (i.e. the relative contribution of the second term T^2/BA^* in Eq. (36)), while the bending/shear part is equal to the 45.23% (i.e. the relative contribution of the third term $2MT/B\sqrt{A^*D}$ in Eq. (36)). When the E_{xx}/G_{xy} ratio is relatively high (as in the case of common laminates) and the laminate is slender, not only the shearing effects have to be taken into account, but all the coupling effect between the shear force and bending moment is to be considered. For an isotropic material with $E_{xx}/G_{xy} = 2.6$, the relative shear term

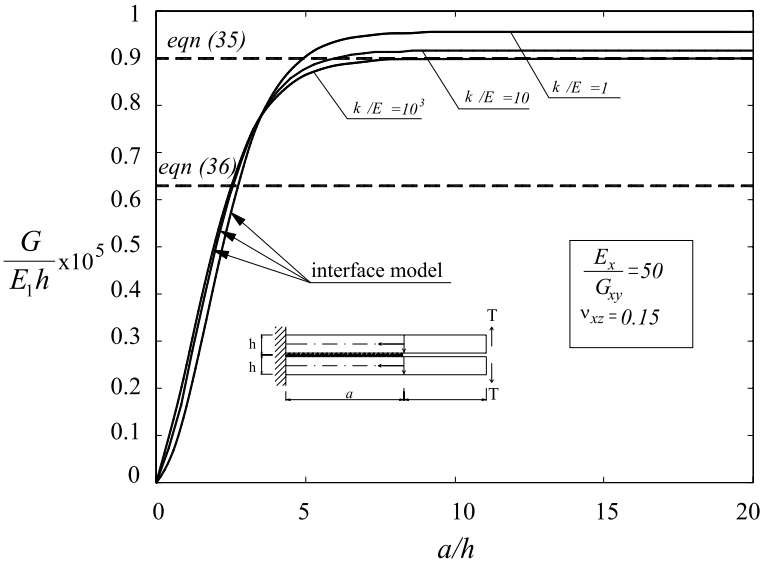

Fig. 18. Energy release rate for various a/h ratios: influence of shear.

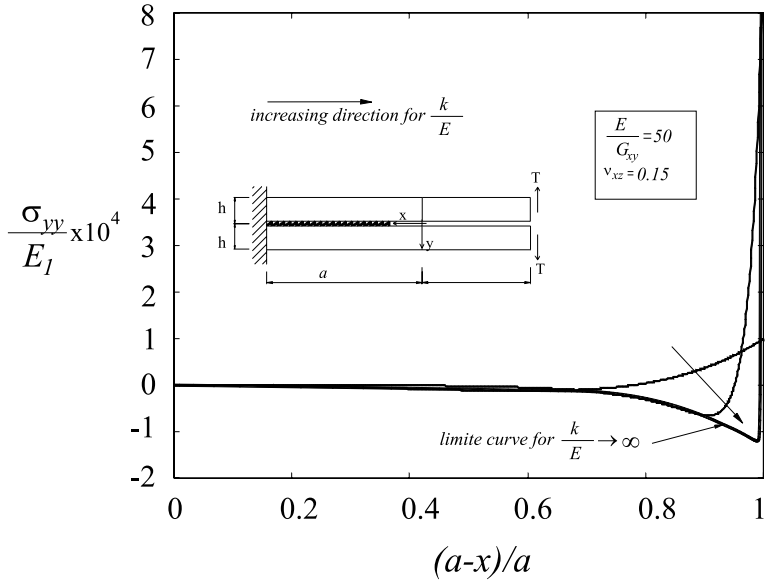

Fig. 19. Interlaminar normal stresses as a function of the interface penalty parameter k.

contribution becomes 0.27%, while the coupling term relative contribution is 10.26%. Note that for the isotropic material the ratio between coupling and shear term increases being proportional to G_{xy}/E_{xx} whereas the absolute contribution of shear and coupling terms decreases.

This important effect may be appreciated only if an improved beam-plate model that includes the shear deformation effects through a layer-wise kinematics is used. In fact, when the shear effects are recovered only by equilibrium conditions (see e.g. Williams (1988), where in the context of the classical beam theory the term due to shear effects in energy release rate is obtained) no coupling effects emerge. It can be observed from Fig. 19 that the interlaminar normal stresses tend towards a non null function (i.e. $\psi_1(0)\sqrt{A^*/D}\exp(-\sqrt{A^*/D}x)$) with a singularity at the crack tip. This is due to the behaviour of the section rotation function ψ_1.

4.2. Complete solution of the two-layer plate model

With procedure similar to that employed in Section 3.1, the system (30) is reduced to a first order differential system coupled with an algebraic eigenvalues problem, $\boldsymbol{y}' = \boldsymbol{A}\boldsymbol{y}$. In this case we set $\boldsymbol{y} = \{u_1, u_1', u_2, u_2', w_1, w_1', w_2, w_2', \psi_1, \psi_1', \psi_2, \psi_2'\}^{\mathrm{T}}$ and $\boldsymbol{A}$ is a 12×12 matrix whose nonzero components are given in Appendix D.

It follows that the matrix of eigenvalues, for sufficiently high values of the penalty parameter k takes the form:

$$\boldsymbol{\Lambda} = \mathrm{diag}\{\alpha, -\alpha, \beta, -\beta, \gamma, -\gamma, 0, 0, 0, 0, 0, 0\},$$

where α, β, γ are real numbers. In the case when the boundary conditions are expressed in the form $\boldsymbol{U}\boldsymbol{c} = \boldsymbol{f}$ we set

$$\boldsymbol{f} = \left\{0, \frac{N_1}{A_1}, 0, \frac{N_2}{A_2}, 0, \frac{T_1}{A_1^*}, 0, \frac{T_2}{A_2^*}, 0, \frac{M_1}{D_1}, 0, \frac{M_2}{D_2}\right\}^{\mathrm{T}},$$

and $\boldsymbol{U}$ is a 12×12 matrix collecting the boundary conditions (given in the Appendix E).

The solution of $\boldsymbol{y}' = \boldsymbol{A}\boldsymbol{y}$ can be found by a linear combination of the particular integrals:

$$\boldsymbol{y} = \sum_{j=1}^{12} c_i \boldsymbol{u}_i \mathrm{e}^{\lambda_i x},$$

where $\boldsymbol{u}_i$ and λ_i are the eigenvectors and eigenvalues of $\boldsymbol{A}$, respectively. If we assume that the plate has high a/h_i ratios, the eigensolutions with positive real part can be excluded from the solution because the constants c_i must vanish otherwise they cause instability of the solution for very large k values. It is worth mentioning that exclusion of the positive eigenvalues is possible only under the above-mentioned assumption (i.e. for high a/h_i ratios) in the context of Reissner–Mindlin kinematics assumptions, while it follows directly as a consequence of the behaviour of the eigenvalues for increasing values of the stiffness parameter in the case of the Kirchhoff kinematics and thus, in the latter case, it does not depend on the length of the uncracked plate. On the other hand, the kinematics assumed in this paragraph coupled with a linear interface model leads to a shear deformable layer-wise laminate model which is able to recover a more actual behaviour of interlaminar stresses. To give a better understanding of the meaning of shear effects occurring in energy release rate evaluation the following considerations based on the J-integral concept are given.

Evaluating the J-integral along a closed path with vertical segments behind and ahead the delamination tip similar to that shown in Fig. 17, and using stresses and strains predicted by the present model leads to the following expression for energy release rate:

$$G = \oint_C \left[\frac{1}{2}\left(\frac{1-\upsilon_{zx}\upsilon_{xz}}{E_x}\sigma_x^2 + \frac{\sigma_{xy}^2}{G_{xy}}\right) - \sigma_{xy}\frac{\partial u}{\partial y}\right]\mathrm{d}y = \oint_C \left[\frac{1}{2}\left(\frac{N_i}{Bh_i} + \frac{12M_i}{Bh_i^3}y\right)^2 - \frac{T_i}{Bh_i}\psi_i\right]\mathrm{d}y. \tag{40}$$

Eq. (40) can be rewritten in the more convenient following form:

$$G = \frac{1}{2}\left[\left[\frac{N_i^2}{A_i} + \frac{M_i^2}{D_i} + \frac{T_i^2}{A_i^*} - 2T_i\psi_i\right]\right]_1 + \frac{1}{2}\left[\left[\frac{N_i^2}{A_i} + \frac{M_i^2}{D_i} + \frac{T_i^2}{A_i^*} - 2T_i\psi_i\right]\right]_2, \tag{41}$$

where $[\![\cdot]\!]_i$ ($i = 1$ for the upper layer and $i = 2$ for the lower one) indicates the jump of the enclosed quantity across the delamination tip section of the ith layer, evaluated as the difference between the value of the enclosed quantity taken behind and ahead the delamination tip. Eq. (41) evidences how energy release rate arises from stress resultant discontinuities.

It can be noted from Eq. (41), that G contains in addition to standard shear terms arising from the jumps of T_i^2/A_i^* terms, coupling terms related to the jump of the quantity $T_i\psi_i$ which may have a notable influence in energy release rate. These terms are neglected in models usually used in literature (see the discussion of analytical methods of fracture energies determination in Allix and Corigliano (1996) or the specialization of the analytical formula found in Cochelin and Potier-Ferry (1991) for G to the present one-dimensional case) in which shear effects are circumscribed only to T_i^2/A_i^* terms. The $T_i\psi_i$ terms generalize the bending shear coupling term introduced in Eq. (36). In fact, it can be easily proved that these terms specialize to $2MT/B\sqrt{A^*D}$ for the scheme considered in Section 4.1.

Obviously, coupling terms vanish both if shear stresses are recovered from equilibrium considerations within the classical plate theory and if a standard shear deformation plate theory is used to model the whole laminate.

A higher order plate theory was proposed by Armanios and Rehfield (1988), which although may provide a good estimate of shear interlaminar stresses is not able to capture the coupling terms since a linear strain distribution is imposed through the thickness of the laminate.

Utilizing the proposed delamination model leads emphasizing that the coupling terms arise from the delamination front discontinuity in stress resultant work and emerge only when section rotation ψ_i is allowed to be discontinuous across the interface. These terms enhance accuracy in energy release rate prediction, since they capture a more actual deformation mechanism at the crack tip in comparison with other models utilized in the literature.

The need to introduce a correction in energy release rate removing the built-in assumption used in double cantilever beam schemes utilized in delamination tests, in order to accurately experimental data, was also discussed by Williams (1989).

The behavior of energy release rate can be also interpreted by referring to the asymptotic orders of singularity of interlaminar stresses at the crack tip when the penalty parameter approaches infinity. Denoting by $\sigma^M_{yy,yx}$ and $\sigma^N_{yy,yx}$ interlaminar stresses produced by bending and axial loading at the crack tip, respectively, (i.e. arising from M_1, M_2, and N_1, N_2 respectively) and by $\sigma^T_{yy,yx}$ interlaminar stresses arising from shear loading (i.e. T_1, T_2), by superposition, the total interlaminar stress is

$$\sigma_{yy,yx} = \sigma^M_{yy,yx} + \sigma^N_{yy,yx} + \sigma^T_{yy,yx}. \tag{42}$$

Now suppose the following asymptotic expansions for interlaminar stresses:

$$\begin{aligned} \sigma^M_{yy,yx} &= \mathrm{O}(k^\alpha) + \mathrm{o}(k^\alpha) \quad k \to \infty, \\ \sigma^N_{yy,yx} &= \mathrm{O}(k^\beta) + \mathrm{o}(k^\beta) \quad k \to \infty, \\ \sigma^T_{yy,yx} &= \mathrm{O}(k^\gamma) + \mathrm{o}(k^\gamma) \quad k \to \infty, \end{aligned} \tag{43}$$

where $\mathrm{O}(k^m)$ is referred to terms of k^m order and $\mathrm{o}(k^m)$ is referred to terms which go to infinity slower than k^m, as $k \to \infty$.

By using the conditions that interface strain energy density must remain bounded at the crack tip as $k \to \infty$, i.e.

$$G = \lim_{k\to\infty} \frac{1}{2K}(\sigma^2_{yy} + \sigma^2_{yx}) = \mathrm{O}(k^0), \tag{44}$$

and that all loading conditions contribute to energy release rate, comparing Eqs. (43) and (44) leads to the following asymptotic orders:

$$\alpha = \beta = \gamma = 1/2. \tag{45}$$

On the other hand, if a classical plate theory is used to model layers, application of J-integral (i.e. utilizing Eq. (40) and neglecting shear stress contribution) easily shows that no shear terms arise in energy release rate, and this leads to the condition

$$\gamma < 1/2,$$

since from Eq. (44) all energy release rate terms G^T containing contribution from $\sigma^T_{yy,yx}$ must satisfy the relation

$$G^T = \mathrm{O}(k^s) \quad \text{as } k \to \infty,$$

with $s < 0$. The introduction of a first order shear deformable kinematics for layers, in fact, modifies the order of interlaminar stresses γ arising from shear loading conditions.

Thus, contrary to the case in which the classical plate theory is used to model the layers, within the proposed Reissner–Mindlin model the interlaminar stresses $\sigma^{T}_{yy,yx}$ yield a non zero contribution to energy release rate both in the form of pure shear terms (i.e. terms such as $\sigma^{T2}_{yy,yx}/k$) and in the form of coupled terms (i.e. terms like $\sigma^{M}_{yy,yx}\sigma^{T}_{yy,yx}/k$ or $\sigma^{N}_{yy,yx}\sigma^{T}_{yy,yx}/k$). In particular, bending/shear coupling terms are related to mixed products between interlaminar stresses such as $\sigma^{M}_{yy,yx}\sigma^{T}_{yy,yx}/k$.

4.3. Numerical examples

The behaviour of the total energy release rate G and of its mode components G_{I} and G_{II} both in the case of Kirchhoff and Mindlin plate models are presented in Fig. 20 where a logarithmic (base 10) scale is used for the horizontal axis. Energy release mode components are evaluated by using Eq. (2). A two-layer plate system with different materials and thickness, loaded with two opposite vertical forces is analysed by using the following parameters:

$$a = 10\ \text{mm},\ h_1 = 1\ \text{mm},\quad E_1 = 93\,800\ \text{MPa},\quad \ell = 10\ \text{mm},\quad B = 10\ \text{mm},\quad T = 50\ \text{N}.$$

It can be noted from Fig. 20 that the total energy release rate G predicted is much higher for Mindlin than for Kirchhoff kinematics, due to shear and coupling terms arising from shear effects. Moreover, we may note that the higher difference between results from Eqs. (23) and (24) and the interface model with shear deformable layers is in mode I component evaluation, because the effect of the additional energy terms comes into play more than the mode II, less activated. Moreover, also in this case the hypothesis that two opposite moments lead activate only mode I component (see Williams, 1988) refers to a simplified model.

An example of two-layer plate system is presented in Fig. 21, where layers of different thickness are loaded with two equal vertical forces and two opposite axial forces. The following parameters are employed:

$$a = 10\ \text{mm},\ h_1 = 1\ \text{mm},\ E_1 = 93\,800\ \text{MPa},\ \ell = 10\ \text{mm},\ B = 10\ \text{mm},\ T = 50\ \text{N},\ N = 100\ \text{N}.$$

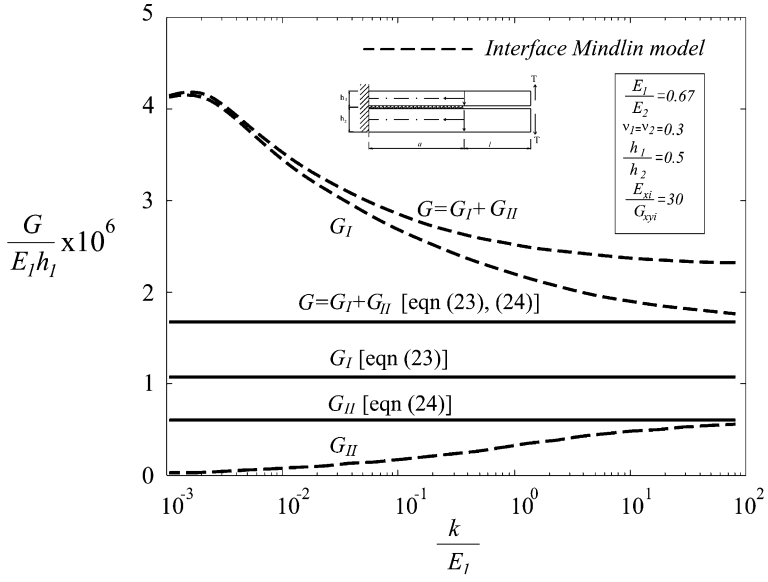

Fig. 20. Energy release rate for a two-layer plate system subjected to vertical forces (mode I prevalent loading).

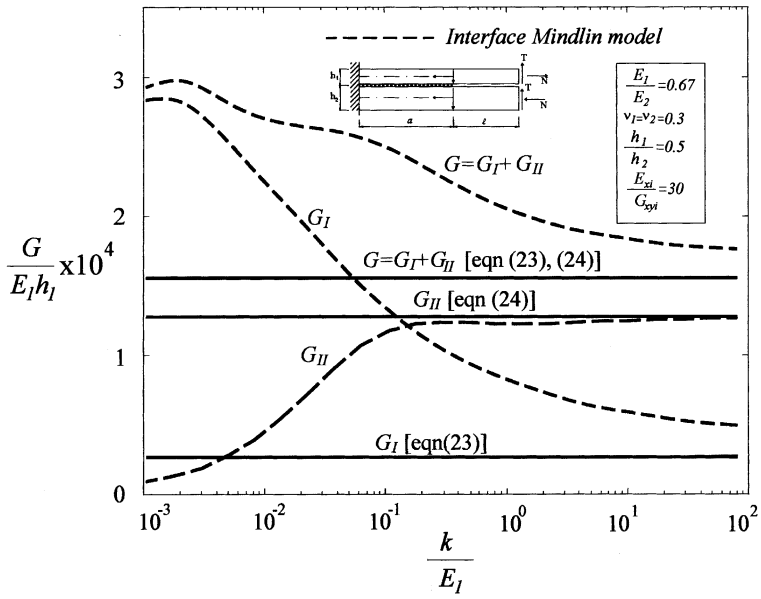

Fig. 21. Energy release rate comparison a two-layer plate system subjected to vertical and axial forces (mode II prevalence loading).

In this case the difference for mode I component is less evident due to the prevalence of mode II component.

5. Conclusions

The delamination problem in layered plates has been analysed by using an interface model and appropriate kinematics models for layers, to achieve an accurate energy release rate evaluation.

The adhesion between layers has been modelled by means of an interface model whose linear constitutive law relates interlaminar stresses acting in the opening and sliding directions with jump of displacements at the interface. This model is useful to capture the salient features of delamination failure. These are

- the estimation of interlaminar stress singularities arising from different kinematics models for layers;
- the influence of bending, shear and axial loads on energy release rate evaluation;
- the influence of shear deformability on plate delamination;
- the mechanical behavior of a laminate due to the presence of interfaces and interlaminar defects.

Moreover, the presented model could become powerful in the context of employment in general two-dimensional plate problems, where a general interface model able to transfer opening, sliding and tearing interlaminar stresses could be introduced to predict local mode components of energy release rate at the delamination front generalizing the present one-dimensional model. This can be done by using a penalty technique similar to that here presented to compute local energy release rate mode components.

As in the present one-dimensional model, this extension, which can be effectively performed through FE analyses, is believed able to capture more accurately shear effects by adopting a layer-wise plate model in which interface elements ensure interlaminar displacement continuity. As pointed out in this work, the use

of a single plate element to model the undelaminated portion of the laminate is not appropriate to capture actual shear effect, since the shear coupling terms, which have a notable bearing on energy release evaluation, are completely neglected.

The analysis has been carried out by modelling the delaminated plate with a layer-wise kinematics using both Kirchhoff and Mindlin plate models for layers. The former approach yields a closed-form energy release rate partition. Employing the latter model gives a refined solution for energy release rate evaluation, from which the significant influence of shear deformability may be evaluated. In particular, for the Mindlin plate model, a main result is that the accurate calculation of energy release rate mode components is due to the inclusion of additional energy terms arising from interaction between shear and normal stresses. As a consequence, these terms modify the order of singularity of interlaminar stresses related to shear loading conditions.

In addition, the mode partition of the energy release rate has been investigated by using an improved layered plate model incorporating interface elements, thus providing a contribution to the clarification of the influence of the stress field on the delamination process. Some comparisons with other results available in the literature, show that mode partition depends on the assumption made to reconstruct interlaminar stress which are not introduced directly in common plate theories but are here determined by introducing an interface model. Mode partition, in fact, is a three-dimensional problem and, in principle, a continuum analysis should give more accurate results than an analysis derived from plate models. Unfortunately, an analysis incorporating exactly local effects is not convenient in practical delamination cases, due to its high computational cost and may involve some difficulties related to the convergence behavior of numerical procedures and to the classical oscillatory stress singularities. Moreover, local analyses are available in the literature only with reference to simplified schemes, the most common being the semi-infinite crack, which are valid, strictly speaking, only when the effect of edge shear resultants is not considered. Thus a refined plate model such as that here proposed can be an effective approach avoiding the need for local analysis and convergence problems of energy release rates by the use of plate variables. Moreover, due to its remarkable simplicity, it provides useful analytical formulas for energy release rate evidencing the main quantities governing delamination behaviour, and some approximations introduced in delamination models widely adopted in the literature.

Finally, the proposed model, although based on simplifying assumptions, is useful to bring out the salient features of the complex delamination problem in multi-layered plates and can represent a powerful tool for most engineering applications. Obviously, the accuracy of mode partition is strongly influenced by an appropriate estimation of interlaminar stresses. As a consequence, it is reasonable to think that the accuracy of mode partition can be improved by using higher order plate theories or by modelling layers by more than one sublaminate. In fact, these models are able to transfer a more refined interlaminar stresses distribution. This issue will be object of future investigations.

The main point of this paper is to highlight the efficacy of the proposed interface approach, which, independently of plate modelling, provides a direct and self-consistent method to determine energy release rate and its mode partition.

Appendix A

Extracting the opportune boundary conditions from Eq. (10), with the notation

$$\frac{M_1 - M_2}{D} = m \quad \text{and} \quad \frac{T_1 - T_2}{D} = t,$$

coefficients c_i can be written as

$$\begin{cases} c_1 = \dfrac{[\alpha m + 2\alpha m\,\mathrm{e}^{2\alpha a} + t\,\mathrm{e}^{2\alpha a} + \alpha m\,\mathrm{e}^{2\alpha a}\cos(2\alpha a) + t\,\mathrm{e}^{2\alpha a}\cos(2\alpha a) - \alpha m\,\mathrm{e}^{2\alpha a}\sin(2\alpha a)}{2\alpha^3[1 + 4\mathrm{e}^{2\alpha a} + \mathrm{e}^{4\alpha a} + 2\mathrm{e}^{2\alpha a}\cos(2\alpha a)]} \\ c_2 = \dfrac{[\alpha m - t - t\,\mathrm{e}^{2\alpha a} - \alpha m\,\mathrm{e}^{2\alpha a}\cos(2\alpha a) - \alpha m\,\mathrm{e}^{2\alpha a}\sin(2\alpha a) - t\,\mathrm{e}^{2\alpha a}\sin(2\alpha a)}{2\alpha^3[1 + 4\mathrm{e}^{2\alpha a} + \mathrm{e}^{4\alpha a} + 2\mathrm{e}^{2\alpha a}\cos(2\alpha a)]} \\ c_3 = -\dfrac{\mathrm{e}^{2\alpha a}[2\alpha m + \alpha m\,\mathrm{e}^{2\alpha a} + \alpha m\cos(2\alpha a) - t - t\cos(2\alpha a) + \alpha m\sin(2\alpha a)]}{2\alpha^3[1 + 4\mathrm{e}^{2\alpha a} + \mathrm{e}^{4\alpha a} + 2\mathrm{e}^{2\alpha a}\cos(2\alpha a)]} \\ c_4 = \dfrac{\mathrm{e}^{2\alpha a}[\alpha m\,\mathrm{e}^{2\alpha a} + t\,\mathrm{e}^{2\alpha a} - \alpha m\cos(2\alpha a) + t - t\sin(2\alpha a) + \alpha m\sin(2\alpha a)}{2\alpha^3[1 + 4\mathrm{e}^{2\alpha a} + \mathrm{e}^{4\alpha a} + 2\mathrm{e}^{2\alpha a}\cos(2\alpha a)]} \end{cases}.$$

Appendix B

The coefficients in Eq. (18) are

$$\begin{cases} c_1 = s \\ c_2 = \dfrac{2\beta n - \mathrm{e}^{\beta a} hs}{2\beta^2(1 + \mathrm{e}^{2\beta a})} \\ c_3 = -\dfrac{\mathrm{e}^{\beta a}(2\beta n\mathrm{e}^{\beta a} + hs)}{2\beta^2(1 + \mathrm{e}^{2\beta a})} \end{cases}$$

where

$$s = -\frac{T_1 + T_2}{D} \quad \text{and} \quad n = \frac{N_1 - N_2}{A} + \frac{h(M_1 + M_2)}{2D}.$$

Appendix C

The ineffective loading system is defined by the following quantities:

$$M_1^a = \frac{D_1(D_2h_1^2(2M + h_1N) + D_1h_2^2(2M - Nh_2))}{2(D_2^2h_1^2 + D_2^2h_2^2) + 2D_1D_2(2h_1^2 + 2h_2^2 + 3h_1h_2)},$$

$$M_2^a = \frac{D_2}{D_1}M_1^a,$$

$$N_1^a = \frac{6D_1D_2(h_1 + h_2)M + D_1(3D_2h_1^2 + 3D_2h_1h_2 + (D_1 + D_2)h_2^2)N}{D_2(4D_1 + D_2)h_1^2 + 6D_1D_2h_1h_2 + D_1(D_1 + 4D_2)h_2^2},$$

$$N_2^a = N - N_1^a.$$

The assumption that the pure mode I condition is represented by two moments which produce the same strain at the crack tip, leads to:

$$M_2 = \bar{\alpha}M_1, \tag{46}$$

where $\bar{\alpha} = -D_2h_1/D_1h_2$. The equivalent stress system in the sense of energy release rate evaluation is thus obtained from Eq. (21) (with $N_1 = 0$) and the equilibrium equations for this particular loading system to recover the global stresses M and N. The parameter α can be obtained from the ratio between M^l and M^u:

$$\alpha = \frac{\bar{\alpha} M_1 - M_2^a}{M_1 - M_1^a},$$

leading to Eq. (27).

Parameter $\bar{\beta}$, the dual of $\bar{\alpha}$, i.e. defined by $M_2 = \bar{\beta} M_1$, which gives only mode II energy release rate can be obtained from the mode II equivalent loading system M_{II}^u, $M_{\mathrm{II}}^l = \beta M_{\mathrm{I}}^u$, $N_{\mathrm{II}}^* = \frac{2(1+\beta)}{h_1+h_2} M_{\mathrm{II}}^u$ by using Eq. (21):

$$\bar{\beta} = \frac{D_2 \left[D_2 h_1^2 + D_1 h_2 (3h_1 + 4h_2) \right]}{D_1 \left[D_1 h_2^2 + D_2 h_1 (4h_1 + 3h_2) \right]}.$$

Appendix D

The nonzero components of the 12×12 matrix $\boldsymbol{A}$ introduced in Section 3.1 are

$$A_{1,2} = 1,\ A_{2,1} = \frac{k}{A_1},\ A_{2,3} = -\frac{k}{A_1},\ A_{2,9} = \frac{kh_1}{2A_1},\ A_{2,11} = \frac{kh_2}{2A_2},\ A_{3,4} = 1,\ A_{4,1} = -\frac{k}{A_2},\ A_{4,3} = \frac{k}{A_2},$$

$$A_{4,9} = -\frac{kh_1}{2A_2},\ A_{4,11} = -\frac{kh_2}{2A_2},\ A_{5,6} = 1,\ A_{6,5} = \frac{k}{A_1^*},\ A_{6,7} = \frac{k}{A_1^*},\ A_{6,10} = -1,\ A_{7,8} = 1,$$

$$A_{8,5} = -\frac{k}{A_2^*},\ A_{8,7} = \frac{k}{A_2^*},\ A_{8,12} = -1,\ A_{9,10} = 1,\ A_{10,1} = \frac{kh_1}{2D_1},\ A_{10,3} = -\frac{kh_1}{2D_1},\ A_{10,6} = \frac{A_1^*}{D_1},$$

$$A_{10,9} = \frac{A_1^*}{D_1} + \frac{kh_1^2}{4D_1},\ A_{10,11} = \frac{kh_1 h_2}{4D_1},\ A_{11,12} = 1,\ A_{12,1} = \frac{kh_2}{2D_2},\ A_{12,3} = -\frac{kh_2}{2D_2},\ A_{12,8} = \frac{A_2^*}{D_2},$$

$$A_{12,9} = \frac{kh_1 h_2}{4D_2},\ A_{12,11} = \frac{A_2^*}{D_2} + \frac{kh_2^2}{4D_2}.$$

Appendix E

The boundary conditions matrix $\boldsymbol{U}$ has the following representation:

$$\boldsymbol{U} = \begin{bmatrix}
u_{1,1}\,\mathrm{e}^{\lambda_1 a} & \dots & u_{1,6}\,\mathrm{e}^{\lambda_6 a} & u_{1,7} & \dots & u_{1,12}a^5 \\
u_{2,1} & \dots & u_{2,6} & u_{2,7} & \dots & 0 \\
u_{3,1}\,\mathrm{e}^{\lambda_1 a} & \dots & u_{3,6}\,\mathrm{e}^{\lambda_6 a} & u_{3,7} & \dots & u_{3,12}a^5 \\
u_{4,1} & \dots & u_{4,6} & u_{4,7} & \dots & 0 \\
u_{5,1}\,\mathrm{e}^{\lambda_1 a} & \dots & u_{5,6}\,\mathrm{e}^{\lambda_6 a} & u_{5,7} & \dots & u_{5,12}a^5 \\
u_{6,1} + u_{9,1} & \dots & u_{6,6} + u_{9,6} & u_{6,7} + u_{9,7} & \dots & 0 \\
u_{7,1}\,\mathrm{e}^{\lambda_1 a} & \dots & u_{7,6}\,\mathrm{e}^{\lambda_6 a} & u_{7,7} & \dots & u_{7,12}a^5 \\
u_{8,1} + u_{11,1} & \dots & u_{8,6} + u_{11,6} & u_{8,7} + u_{11,7} & \dots & 0 \\
u_{9,1}\,\mathrm{e}^{\lambda_1 a} & \dots & u_{9,6}\,\mathrm{e}^{\lambda_6 a} & u_{9,7} & \dots & u_{9,12}a^5 \\
u_{10,1} & \dots & u_{10,6}\,\mathrm{e}^{\lambda_6 a} & u_{10,7} & \dots & 0 \\
u_{11,1}\,\mathrm{e}^{\lambda_1 a} & \dots & u_{11,6}\,\mathrm{e}^{\lambda_6 a} & u_{11,7} & \dots & u_{11,12}a^5 \\
u_{12,1} & \dots & u_{12,6} & u_{12,12} & \dots & 0
\end{bmatrix}.$$

References

Allix, O., Corigliano, A., 1996. Modelling and simulation of crack propagation in mixed-modes interlaminar fracture specimens. Int. J. Fract. 77, 111–140.

Allix, O., Ladevéze, P., Corigliano, A., 1995. Damage analysis of interlaminar fracture specimens. Compos. Struct. 31, 61–74.

Armanios, E.A., Rehfield, L.W., 1988. Interlaminar fracture analysis of composite laminates under bending and combined bending and extension. Composite materials: testing and design (eight conference), ASTM STP 972, pp. 81–94.

Ascione, L., Bruno, D., 1985. On the delamination problem of two-layer plates. Proceedings of the Second Meeting on Unilateral Problems in Structural Analysis, Ravello, 22–24 September, 1983, CISM Courses and Lectures no. 288, Springer, Berlin.

Beuth, J.L., 1996. Separation of crack extension modes in orthotropic delamination models. Int. J. Fract. 77, 305–321.

Bigoni, D., Serkov, S.K., Valentini, M., Movchan, A.B., 1998. Asymptotic models of dilute composites with imperfectly bonded inclusions. Int. J. Solids Struct. 35, 3239–3258.

Bruno, D., 1988. Delamination buckling in composite laminates with interlaminar defects. Theoret. Appl. Fract. Mech. 9 (2), 145–159.

Bruno, D., Greco, F., 2000. An asymptotic analysis of delamination buckling and growth in layered plates. Int. J. Solids Struct. 37, 6239–6276.

Bruno, D., Grimaldi, A., 1990. Delamination failure of layered composite plates loaded in compression. Int. J. Solids Struct. 26 (3), 313–330.

Chai, H., 1990. Three dimensional fracture analysis of thin film debonding. Int. J. Fract. 46, 237–256.

Chai, H., Babcock, C.D., Knauss, W.G., 1981. One dimensional modelling of failure in laminated plates by delamination buckling. Int. J. Solids Struct. 17 (11), 1069–1083.

Chang, D.J., Muki, R., Westmann, R.A., 1976. Double cantilever beam models in adhesive mechanics. Int. J. Solids Struct. 12, 13–26.

Chatterje, S.N., Kulkarni, S.V., 1979. Shear correction factors for laminated plates. AIAA J. 17 (5), 498–499.

Cochelin, B., Potier-Ferry, M., 1991. A numerical model for buckling and growth of delaminations in composite laminates. Comp. Meth. Appl. Mech. 89, 361–380.

Davidson, B.D., Hurang, H., Schapery, R.A., 1995. An analytical crack-tip element for layered elastic structures. J. Appl. Mech. 62, 294–305.

Hutchinson, J.W., Suo, Z., 1992. Mixed mode cracking in layered materials. In: Advances in Applied Mechanics, vol. 28. Academic Press, New York.

Hwu, C., Hu, J.S., 1992. Stress intensity factors and energy release rates of delaminations in composite laminates. Eng. Fract. Mech. 42 (6), 977–988.

Kanninen, M.F., 1973. An augmented double cantilever beam model for studying crack propagation and arrest. Int. J. Fract. 9, 83–91.

Larsson, P.-L., 1991. On delamination buckling and growth in circular and annular orthotropic plates. Int. J. Solids Struct. 27 (1), 15–28.

Reddy, J.N., 1986. Applied functional analysis and variational methods in engineering. McGraw-Hill, New York.

Reddy, J.N., Grimaldi, A., 1985. On delamination in plates: a unilateral contact approach. Proceedings of the Second Meeting on Unilateral Problems in Structural Analysis, Ravello, September 22–24, 1983, CISM Courses and Lectures no. 288, Springer, Berlin.

Rice, J.R., 1988. Elastic fracture mechanics concepts for interfacial cracks. ASME J. Appl. Mech. 55, 931–938.

Schapery, R.A., Davidson, B.D., 1990. Prediction of energy release rate for mixed-mode delamination using classical plate theory. Appl. Mech. Rev. 43, S281–S287.

Sih, G.C., 1974. Strain energy density factor applied to mixed mode crack problems. Int. J. Fract. 10, 305–322.

Suo, Z., 1990. Delamination specimens for orthotropic materials. J. Appl. Mech. 57, 627–634.

Suo, Z., Hutchinson, J.W., 1990. Interface crack between two elastic layers. Int. J. Fract. 43, 1–18.

Williams, J.G., 1988. On the calculation of energy release rates for cracked laminates. Int. J. Fract. 36, 101–119.

Williams, J.G., 1989. The fracture mechanics of delamination tests. J. Strain Anal. 24 (4), 207–214.

Yin, W.L., 1985. Axisymmetric buckling and growth of a circular delamination in a compressed laminate. Int. J. Solids Struct. 21 (5), 503–514.

Yin, W.-L., Wang, J.T.S., 1984. The energy-release rate in the growth of a one-dimensional delamination. J. Appl. Mech. 51, 939–941.

Yin, W.L., Sallam, S.N., Simitses, G.J., 1986. Ultimate axial load capacity of a delaminated beam-plate. AIAA J. 24 (1), 123–128.